Radioactivity, radiogenic heat production and environmental radiation risk of the Basement Complex rocks of Akungba-Akoko, southwestern Nigeria: insights from *in situ* gamma-ray spectrometry

Adedibu Sunny Akingboye[1, 5, *], Abimbola Chris Ogunyele[1, 6], Adeleke Teslim Jimoh[1], Oluwatobi Blessing Adaramoye[1], Adedapo Oluwasanu Adeola[2, 3], Toluwaleke Ajayi[4]

[1]*Department of Earth Sciences, Adekunle Ajasin University, P.M.B. 001 Akungba-Akoko, Ondo State, Nigeria*
[2]*Department of Chemical Sciences, Adekunle Ajasin University, P.M.B. 001 Akungba-Akoko, Ondo State, Nigeria*
[3]*Department of Chemistry, University of Pretoria, Pretoria, Lynnwood Road, Hatfield, Pretoria 0002, South Africa*
[4]*Department of Geological Sciences, Ohio University, Athens, United States*
[5]*Current at: Geophysics Section, School of Physics, Universiti Sains Malaysia, 11800 Penang, Malaysia*
[6]*Current at: Department of Earth and Environmental Sciences, University of Pavia, Via Ferrata, 1-27100 Pavia, Italy*
[*]*Corresponding Author: adedibu.akingboye@aaua.edu.ng; **ORCID ID:** https://orcid.org/0000-0003-2195-6098*

Abstract

The Basement Complex rocks of Akungba-Akoko, southwestern Nigeria, typically migmatites (M), biotite gneisses (BGN), granite gneisses (GGN), charnockites (Ch), biotite granites (BG) and pegmatites (P), were assessed using ground gamma-ray spectrometry (GRS). This study aimed at determining rocks' radionuclides concentration, alterations, radionuclides mobilization, radiogenic heat production (RHP) rate (first report for the area) and environmental radiation risk to humans. The results of this study were integrated with previous data on the petrography and geochemistry of these rocks, for detailed interpretation. The results of average elemental and activity concentrations for Akungba-Akoko rocks, were 2.66%, 3.16 ppm and 13.98 ppm, and 831.35, 39.01 and 56.77 $Bqkg^{-1}$ for ^{40}K, ^{238}U and ^{232}Th, respectively; with increasing rock order of Ch < M < GGN < BGN < P < BG. High radionuclides concentration in the rocks, with exception of charnockites, were determined by high fraction of K-feldspar, plagioclase, biotite and accessory minerals – zircon and monazites. On the other hand, the low radionuclides concentration in the rocks, especially in Ch and M, were aided by the variability of the naturally occurring radioactive elements (NORMs) caused by alterations and mobilization during metamorphism and crystallization processes as suggested by radioelements composite, K/eTh ratio and F-parameter of Efimov analyses. RHP average of 2.03 μWm^{-3} above the crustal average range of 0.8 – 1.2 μWm^{-3} may have significantly contributed to the heat flux in the studied area; however, the RHP of charnockites are lower than the crustal range. The absorbed dose rate average of 87.98 $nGy\,h^{-1}$ was within the permissible range, and other estimated radiological parameters, namely annual effective doses, hazard indices, gamma activity and activity utilization index, were all far below the permissible limit of 1 $mSv\,y^{-1}$ for these rocks. However, annual gonad dose equivalent (618.874 $\mu Sv\,y^{-1}$) and excess life cancer risk ($1.511 * 10^{-3}$) were above their permissible limits. Due to the high gamma radiations from the pegmatitic and biotite-rich rocks in the studied area, their high usage should be reduced. Hence, periodic monitoring of the study area is advised.

Keywords: *In situ* gamma-ray spectrometry; rock radioactivity; hydrothermal alteration; radiogenic heat production; environmental radiation risk; Akungba-Akoko.

1. Introduction

Radionuclides in crustal materials are widespread and their abundance can contribute to the levels of background radiation in earth's environment. These background radiations are attributed mainly to primordial radionuclides, especially ^{40}K, ^{238}U and ^{232}Th and their daughter products; with minor contributions from cosmogenic radiations; and human produced radiations from mining, and production and application of fertilizers (e.g. phosphate-rich fertilizers), etc (Abd El-Naby and Saleh 2003; Tzortzis and Tsertos 2004; Akkurt et al. 2010; Cinar et al. 2017). The intensity of these radiations depends on the amount of naturally occurring radioactive minerals (NORMs) present in rocks and soils, and the time of exposure (Al-Trabulsy et al. 2011; Kalyoncuoglu 2015). The radiations have the potential to increase the levels of both outside and inside irradiations and radiological risks to which human beings are exposed to in the environment via ingestion and inhalation (Tzortzis et al. 2003; Faweya et al. 2013; Chandrasekaran et al. 2014). These radiological risks are also linked to the exposure to radioactivity and radon exhalation from natural (Chen et al 2010; Stoulos et al. 2003) and artificial (Bartova et al. 2017; Coletti et al. 2020) building materials.

Prolonged exposure to excess radiations above the safe limits for humans can result to environmental health illnesses, such as cancer of the lung and blood, fever, hair loss, damage of gene pool, mental retardation in children caused by teratogenic exposure to radiation during pregnancy, etc or even death (Avwiri et al. 2011; Uyanik et al. 2013; Rafique et al. 2014; Akpan et al. 2020). In addition, appreciable amounts of radionuclides found in all geologic formations, air and streams/rivers/oceans can also contribute to the earth's internal and terrestrial heat flux (Perry et al. 2006; Clauser 2020). Therefore, terrestrial radiation levels can accurately be determined by measuring the radiations (α-particle, β-particle and γ-ray) emanating from the decay of naturally occurring radionuclides contained in rocks and soils. The gamma radiation is the most useful of all these radiations in radiospectrometry surveys, because it can be measured at several hundreds of metres above the earth's surface. However, the accurate determination of the concentrations of these naturally occurring radionuclides is affected by a number of numerous factors, such as nature and geometry of strata, minerals containing trace amounts of radionuclides (e.g. ilmenite, rutile, zircon, monazite and xenotime), and moisture, etc (Kathren 1998; Narayana et al. 2005; Erbek and Dolmaz 2018).

The gamma-ray spectrometric measurements as a means for geological mapping have been reported in many locations of the world, to assess radionuclide concentrations in crustal formations (El-sadek 2009; Adabanija et al. 2020; El Qassas et al. 2020), in geothermal fields (Saqan et al. 2001; Eggeling et al. 2013), along geologically altered zones (Ramola et al. 2014), in volcanic areas (Rosianna et al. 2020; Cinelli et al. 2020), and in active mining sites (Innocent et al. 2013). Radionuclides also serve as effective geochemical indicators (Wang et al. 2016). The method has been used in lithological and rock alteration characterisation (Maden and Akaryali 2015a; Youssef and Elkhodary 2013; Ademila et al. 2018) and have been effective in the determination of uranium migration in crustal formations (Asfahani et al. 2007; Youssef et al. 2017) as well as crustal radiogenic heat production (Youssef 2016; Hasterok and Webb 2017; Sabra et al. 2019).

Over the years, similar researches have been conducted in southwestern Nigeria (Ademola et al. 2008; Ademola et al. 2014; Oyeyemi, et al. 2017; Ajayi et al. 2018; Adagunodo et al. 2019), but with few researches conducted particularly in and around the study area (Akungba-Akoko) (Ajayi and Ajayi 1999; Ajayi et al. 2006; Akingboye and Ademila 2019). In the study conducted by Ajayi and Ajayi (1999) at different localities within Ondo and Ekiti States, Nigeria, topsoil samples were analysed using Canberra Series 10 Plus multichannel analyzer to assess the exposure rate from environmental gamma radiations. From the one hundred and eighty-six topsoil samples taken, only five representative samples were collected from Oka-Akoko, Ondo State; a neighbouring town to Akungba-Akoko. The derived results from the few analysed topsoil samples therefore suffer limitation of not giving the spatial radionuclide distribution as baseline for radiologic assessment for surrounding towns. Akingboye and Ademila (2019) employed gamma-ray spectrometric method to determine the distribution of *in situ* radionuclides in granite gneissic rocks with residual topsoils as well as estimated the radiological hazards on humans within Akunu-Akoko and Ayere in Ondo and Kogi States, respectively. This study was conducted in faraway localities, and as such the results cannot serve environmental radiation risk threshold for the present study area. In other study, Ajayi et al. (2006) employed Geiger-Muller Counter to determine the spatial radioactivity levels of basement rocks in Akoko area of Ondo State, Nigeria. The employed instrument suffers limitations, such as measuring effectively radiation in the range of beta particle and can only be accurately deployed in ground survey over

terrain with little soil cover. Besides these shortcomings, not all rocks in the studied area were investigated for radiological threats. Since all the methods employed around and within Akungba-Akoko area suffered from one limitation or another coupled with its paucity of data on radioactivity and radiological hazard assessments of *in situ* rocks; hence, a comprehensive study is highly needed to forestall any radiological health threats on the people residing in this area.

In light of the above, we carried out a detailed real-time *in situ* gamma-ray spectrometric assay measurements to determine the natural radioactivity and associated radiological hazards of the Basement Complex rocks in Akungba-Akoko, southwestern Nigeria. This study integrated existing petrographic and geochemical data of the studied rocks with measured rocks' radionuclides concentration and estimated radiological parameters. The specific objectives of this study, therefore, include the determination of the spatial distribution of radionuclides, lithological alterations characterisation, radionuclides mobilization, and distribution of radiogenic heat production (first report for the area), as well as providing environmental radiation risk report to know if the study area is radiologically safe or not. This study is expected to serve as baseline for referencing radionuclide concentrations and radiological standards for future monitoring in Akoko communities and elsewhere.

2. Location and Geological Setting

Akungba-Akoko lies in the northern part of Ondo State, southwestern Nigeria, between latitudes 07^{o}26' and 07^{o}30' N and longitudes 005^{o}42' and 005^{o}46' E, and the area is underlain by the Precambrian Basement Complex rocks of southwestern Nigeria (Figs. 1 and 2). The Precambrian Basement Complex of Nigeria is located within the Pan-African Trans-Saharan mobile belt between the West African and Congo Cratons and to the south of the Tuareg Shield (Woakes et al. 1987; Kroner et al. 2001; Goodenough et al. 2014) (see top right map in Fig. 1). The complex comprises three major lithological groups, namely; the Migmatite-Gneiss Complex, the Schist Belts and the Older Granites which intrude the former two groups.

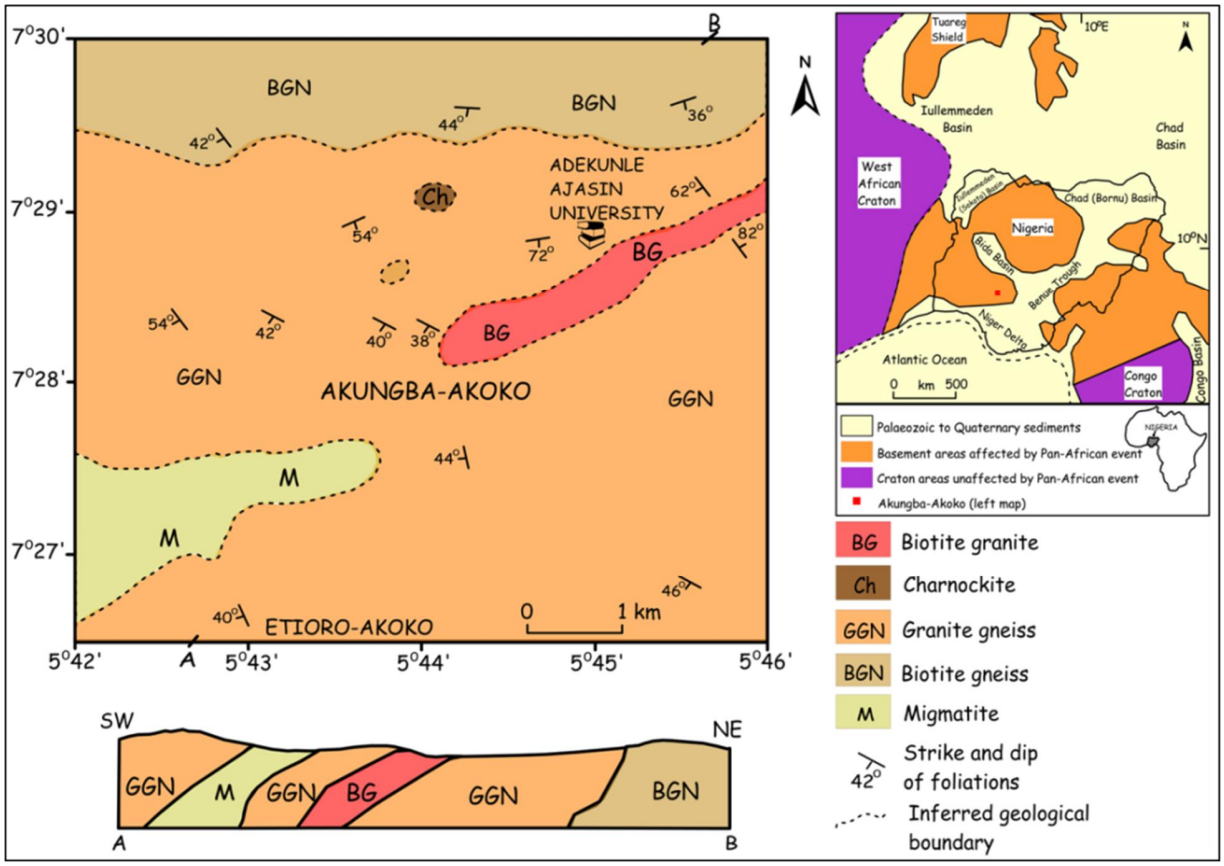

Fig. 1: Geological map of Akungba-Akoko area (modified after Ogunyele et al. 2019). Regional geological map of Nigeria (top right map) showing the study area (modified after Woakes et al. 1987).

The lithological units in the study area comprise the Migmatite-Gneiss Complex (MGC) rocks of the southwestern Nigeria, which are intruded by the Pan-African Granitoids (Rahaman 1989; Ogunyele et al. 2019) (Fig. 1). The MGC rocks in the area include migmatites, granite gneisses and biotite gneisses. Granite gneiss is the predominant rock covering over 85% of the area. It is light grey, medium to coarse grained and weakly to moderately foliated, with light- and dark-coloured bands. The biotite gneiss occurs as ridges in the northern part of the area and extends to Ikare area and other adjoining towns. An enclave of the biotite gneiss also occurs within the granite gneiss. The migmatite formed a ridge which comprises all the rock types, except charnockite, and it extends from southwestern part of Akungba to Supare area in an ENE-WSW direction. All the MGC rocks show evidence of different structural features, such as folds, joints and faults. The granite is medium to coarse grained. The coarse grained, dark-coloured

charnockite with a shining appearance occurs as a core in the granite gneiss and as boulders. Quartz veins and intrusives, such as pegmatite, aplite, and basic dykes and sills also occur within the MGC rocks of Akungba-Akoko.

The mineralogy (as observed in thin sections and hand specimens) of the rocks in the study area comprises quartz + K-feldspar + plagioclase feldspar + biotite ± hornblende + muscovite ± garnet ± pyroxene + opaque minerals. In terms of major element geochemistry, these rocks are composed largely of SiO_2 of over 57.5%, Al_2O_3 is $\leq$ 17.9%, with subordinate amounts of TiO_2, Fe_2O_3, MnO, MgO, CaO, Na_2O, K_2O, and ± P_2O_5, are below 7.2% (Ogunyele et al. 2019). Using the whole-rock geochemical data from the Akungba-Akoko rocks, Ogunyele et al. (2019) discriminated the biotite- and granite gneisses as medium-K calc-alkaline, ferroan rocks; and the biotite granites and charnockites as high-K calc-alkaline, magnesian rocks. The study also revealed that the granite gneisses are S-type peraluminous granitoids while the biotite gneisses, biotite granites and charnockites display I-type affinity. The study concluded that the gneisses are orthogneisses formed by metamorphism of igneous protoliths of granitic composition while the biotite granites and charnockites are of igneous/magmatic origin. The biotite granites, charnockites and the igneous protolith of the biotite gneisses were formed from magmas derived by partial melting of crustal igneous rocks (or their metamorphic equivalents), whereas the igneous protolith of the granite gneisses was probably derived from partial melting of shallow crustal or (meta-) sedimentary rocks.

3. Methodology

3.1 Gamma-ray Spectrometry Measurement

Ground gamma-ray spectrometry (GRS) method was employed for determining *in situ* concentrations of radionuclides and associated dose rates in crustal rocks in Akungba-Akoko area. NORMs in rocks are of varying amounts and they disintegrate to emit radioactive particles (α-particle, β-particle and γ-ray) at specific ionization levels. These particles are detectable either placing the gamma-ray spectrometer directly in contact with the surface of the materials or at an average height of 1 m above them. For the purpose of this study, the former approach was used to assess the gamma radiations from rocks in the study area.

GRS measurements for this study used a portable hand-held gamma-ray spectrometer (512-channels thallium-activated sodium iodide [NaI(TI)] scintillation detector with crystal size of $2'' * 2''$) made by GF-Instrument Inc., with energy range of 0 – 3 MeV. The instrument is capable of recording the full gamma ray spectrum and can also sum channels over broad energy windows for estimation of K, eU and eTh concentrations. The employed calibration and working principles were based on the recommendation of the International Atomic Energy Agency (IAEA) (1991, 2003). The calibration involves constants associated with the instrument count rates, environmental dose rates, stripping ratios and sensitivity constants. The calibrations have been stored in the memory of this instrument, and the measured values were subtracted from the calibrated factors. The resulting exact values of the measured radionuclides and associated absorbed doses are displayed. This is done to account for the correction of background radiations due to internal radioactivity of the instrument, cosmic and atmospheric radon effects.

In this study, *in situ* measurements on rocks in the area were taken in Spectra and Assay mode. This provides accurate determination of the concentrations of K (%), eU (ppm) and eTh (ppm), and their individual emission and Total Count (TC) emission rates per second (i.e. in cps), as well as associated dose rates. The investigated rocks include migmatites, biotite gneisses, granite gneisses, charnockites, biotite granites and pegmatites. Measurements were taken during the dry season because of the eU- and eTh-migration effects which are often experienced in rainy season (Erbek and Dolmaz 2018). Measurements were acquired at every point where the rocks are exposed. However, some of these rocks were buried by the topsoils, especially around the southwestern part of the studied area. A total number of 523 points were investigated altogether and were indicated in Fig. 2b. On a particular outcrop, two readings were taken each for K (%), eU, eTh, TC and dose rate, and their average values were calculated thereafter. The activity concentrations of ^{40}K, ^{238}U and ^{232}Th in $Bqkg^{-1}$ for these rocks were calculated from their measured elemental concentrations using the conversion factors in Table 1. The results were used to compute the radiological hazards for the area. The resulting radionuclides and radiological hazard results were used to produce different representative maps using Kriging method for data gridding in the Oasis Montaj^{TM} Utility software interface, by employing the dialogue control protocol to automatically determine the cell spacing (i.e. station separations) of the gridded data sets.

The investigated area covers approximately 5.2 km by 5 km to give an approximate area of 26 km^2. The rocks in the area were grouped into different locations based on their occurrence (see Table 2 and Fig 2b). The *Ibaka*, *Ilale* and *Okusa* quarters occupy the western, central and eastern parts of Akungba-Akoko, including the Adekunle Ajasin University, Akungba-Akoko (AAUA) Campus. But the data for AAUA Campus were separated to determine the actual radionuclides activity and their effects on the large population within the campus. The southwestern part is occupied by *Araromi* and *Okele* quarters and a part of Supare-Akoko. Apart from *Akunmi* quarter, *Araromi* quarter still forms part of the southeastern Akungba. The northern axis extends from after AAUA Campus to the southern part of Ikare-Akoko, Ondo State.

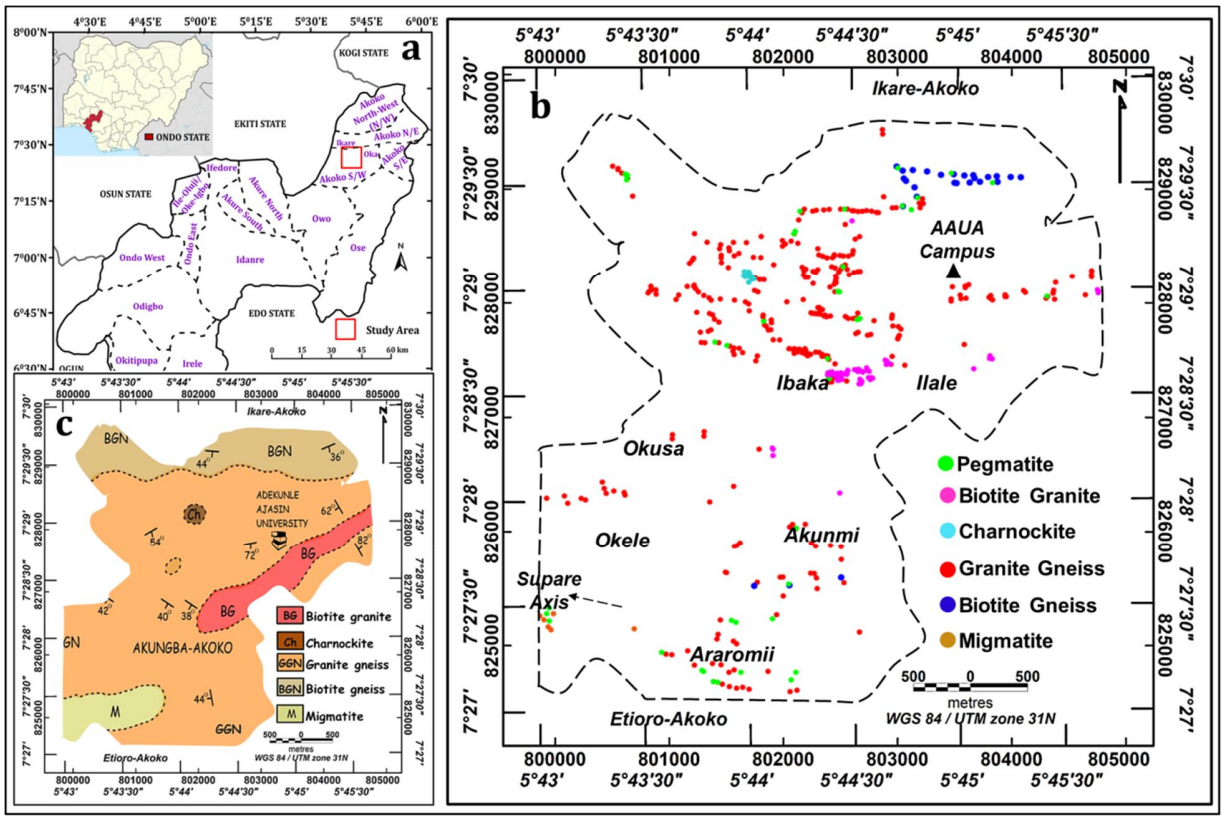

Fig. 2: (a) Location map of Ondo State showing the study area. (b) GRS data acquisition map of Akungba-Akoko showing the localities and measurement points. (c) Sectionalized geological map of Akungba-Akoko showing the exact area investigated.

Table 1: Conversion factors for radionuclide concentrations (in % and ppm) to specific activity concentrations ($Bqkg^{-1}$) (IAEA, 2003).

1% ^{40}K	313 $Bqkg^{-1}$
1 ppm ^{238}U	12.5 $Bqkg^{-1}$
1 ppm ^{232}Th	4.06 $Bqkg^{-1}$

3.2 Calculation of the Radiation Hazard Parameters

The radiological hazards for Akungba-Akoko Basement Complex rocks were computed using various radiation hazard parameters and their equations as follows:

The absorbed dose rate ($\mathcal{D}$) was determined for the amount of radiation energy in air using equation 1 recommended by UNSCEAR (2000), to reaffirm the dose rate values given by the gamma-ray spectrometer. The radium equivalent (Ra_{eq}) for assessing specific activity concentrations in rocks with non-uniformity radiations of ^{40}K, ^{238}U and ^{232}Th and their associated potential risks, was calculated using equation 2 suggested by Beretka and Matthew (1985). The estimation of Ra_{eq} is based on the assumption that 10 $Bqkg^{-1}$ of ^{226}Ra, 7 $Bqkg^{-1}$ of ^{232}Th and 130 $Bqkg^{-1}$of ^{40}K produce the same gamma radiation dose rate (UNSCEAR 1988).

$$\mathcal{D}\ (nGy\ h^{-1}) = 0.0417A_K + 0.462A_U + 0.621A_{Th} \quad (1)$$

$$Ra_{eq}\ (Bqkg^{-1}) = A_U + 1.43A_{Th} + 0.077A_K \quad (2)$$

Where A_K, A_U and A_{Th} are the activity concentrations of ^{40}K, ^{238}U and ^{232}Th in $Bqkg^{-1}$ respectively.

The radioactive heat production (RHP) rate defined as the amount of heat liberated in unit time from a volume of rock during the decay of unstable radioactive elements and their isotopes was estimated using equation 3 given by Rybach (1998). This factor depends on lithological and geochemical properties of rocks (Mareschal et al. 2000; Maden and Akaryali 2015b).

$$A\ (\mu W m^{-3}) = 10^{-5}\rho\ (3.48C_K + 9.52C_U + 2.56C_{Th}) \quad (3)$$

Where ρ is the average rock density in kgm^{-3} and was taken as 2.70 g/cc = 2700 kgm^{-3}, C_K, C_U and C_{Th} are the concentrations of ^{40}K in weight-%, and ^{238}U and ^{232}Th in weight-ppm and weight-ppm (i.e. $10^{-6} kg\ kg^{-1}$), respectively.

To evaluate radiations from air and shielding construction materials which serve as potential to increase radiation exposure to humans, outdoor- and indoor-annual effective dose equivalents indicated as $AEDE_{out}$ and $AEDE_{in}$, respectively, were determined. The outdoor and indoor occupancy factors of 0.2 and 0.8, respectively (UNSCEAR 2000); conversion coefficient factor ($f = 0.7 * 10^{-6}\ Sv\ Gy^{-1}$) for converting absorbed dose in air ($\mathcal{D}$) to AEDE; and indoor/outdoor occupancy time ($\mathcal{T}$) for one year ($24h * 365.25 \cong 8760\ h$), were used as inputs in equation 4 given by UNSCEAR (2000) to derive equations 5 and 6.

$$AEDE\ (mSv\ y^{-1}) = \mathcal{D} * \mathcal{T} * f \quad (4)$$

$$AEDE_{out}\ (mSv\ y^{-1}) = \mathcal{D} * 8760 * 0.2 * 0.7 * 10^{-6} \quad (5)$$

$$AEDE_{in}\ (mSv\ y^{-1}) = \mathcal{D} * 8760 * 0.8 * 0.7 * 10^{-6} \quad (6)$$

In order to account for respiratory dysfunction in humans arising from internal exposure to ^{222}Rn and its radioactive progeny (Beretka and Mathew 1985; Tufail et al. 2007), external and internal radiation hazard indices denoted as RH_{ex} and RH_{in}, respectively, were evaluated using equations 7 and 8, recommended by Ramasamy et al. (2009). To support this, activity concentration index (AC_γ) used for estimating the gamma radiation hazard associated with rocks' radionuclides was also estimated using equation 9 given by European Commission (EC) (1999). EC (1999) suggested that values of $AC_\gamma \leq 2$, $2 \leq AC_\gamma \leq 6$, and $AC_\gamma > 6$ correspond to annual effective doses of 0.3, 1 (as recommended limit), and greater than 1 $mSv\ y^{-1}$ (poses radiological threats), respectively. Similarly, activity utilization index (AUI) was calculated to determine the threat levels from combined radiations of ^{40}K, ^{238}U and ^{232}Th in the rocks using equation 10 given by Ramasamy et al. (2011). Finally, the effects of gamma exposure above safe limits to causing gonads' damage and cancer of the born marrow in humans (UNSCEAR 1988) were determined through annual gonadal dose equivalent (AGDE) and excess lifetime cancer risk (ELCR) using equations 11 and 12, respectively, given by Mamont-Ciesla et al. (1982) and Taskin et al. (2009).

$$RH_{ex} = A_U/370 + A_{Th}/259 + A_K/4810 \leq 1 \quad (7)$$

$$RH_{in} = A_U/185 + A_{Th}/259 + A_K/4810 < 1 \quad (8)$$

$$AC_\gamma = A_K/3000 + A_U/300 + A_{Th}/200 \leq 1 \quad (9)$$

$$AUI = (A_k/500\ Bqkg^{-1})f_k + (A_u/50\ Bqkg^{-1})f_u + (A_{Th}/50\ Bqkg^{-1})f_{Th} \quad (10)$$

$$AGDE\ (\mu Sv\ y^{-1}) = 3.09A_U + 4.18A_{Th} + 0.314A_K \quad (11)$$

$$ELCR = AEDE_{in} * \xi * \mathcal{F} \quad (12)$$

Where f_k, f_u and f_{Th} are given as 0.041, 0.462 and 0.604 as conversion factors for ^{40}K, ^{238}U and ^{232}Th, respectively. ξ is the lifetime expectance (70 years), and $\mathcal{F} = 0.05\ Sv^{-1}$ as cancer risk stochastic factor for the general public (ICRP 1990).

4. Results

4.1 Radioactivity: elemental and activity concentrations and total count emission rate

Several distinct lithologic associations, textural and structural complexities and geochemical alterations can be distinguished from radiospectrometric data sets based on radioactivity signatures. The results of spatial distribution of the measured elemental concentrations of ^{40}K (%), ^{238}U (ppm) and ^{232}Th (ppm) in Akungba-Akoko Basement Complex rocks are shown as Fig. 3a – c, respectively, and are presented in Table 2 showing the rocks' radionuclides for different locations within studied area. In Fig. 3a, rocks at the northern, northwestern corner, eastern, and a large portion of the southern parts of the area show intermediate to high concentration of K% ranging from 2.55% to >5.48%. Rocks around the central part depict low to intermediate concentration of K% in the range <1.80 – 2.5%, with pockets of high concentration responses. Low K% concentration is evinced within the large chunk of high concentration response in the southern part of the area. The exact values of the measured K% concentration ranges from BDL (below detection limit) – 9.58%; eU ranges from BDL – 26.20 ppm while eTh ranges from BDL – 93.70 ppm for different rocks at the respective locations (Table 2). In Fig. 3b, depletion in high eU concentration is witnessed in rocks around the southern part with concentration mainly in the range of BDL – 2.54 ppm. Whereas rocks at the central, northwestern corner and parts of AAUA campus towards the northern axis have high eU ranging from 2.93 – >8.89 ppm. In Fig. 3c, rocks around the southern to central parts of the area depicts very low to moderately high eTh (BDL – 12.99 ppm). The high eTh in the range of 14.40 – >40.38 ppm depicted by rocks around the northern axis, northwestern and eastern corners suggest abundance of highly rich Th-bearing minerals in them. The eU, unlike eTh and K, is actively mobilized in oxidizing environment and

easily leached by groundwater. Whereas eTh is relatively stable in the oxidation zone and stay in place under oxidizing conditions leading to the alteration of the original U-Th state (Chandrasekaran et al. 2014). It is worth to note that pockets of high radionuclides signature seen in all the maps are the sections mostly dominated by pegmatites.

The TC map (Fig. 3d), on the other hand, shows the combined emission rate from these three radionuclides per second. High spontaneous radioactive emission with values >361 cps is observed around the northern axis, northwestern and eastern to southeastern parts of the study area. This suggests high fraction of NORMs from abundance of biotite and potassic feldspar in the biotite- and feldspar-rich rocks. Similarly, sub-rounded and patches to trend-like high emission responses are also seen at the southwestern axis and central, respectively. Other parts of the map show very low – moderate emission rates in the range of <342 – 360 cps for these radionuclides. In Table 2 showing the measured TC rates for the rocks and their estimated averages, the granite gneisses around the Akungba north emit the lowest radioactivity rate of 309.30 cps, while the pegmatites around AAUA Campus emit the highest (440.90 cps) total radiation. Other rock types exhibit varying emission rates between these two values. However, based on estimated averages, the TC averages for the rocks in the studied area ranges between 331.82 (Ch around Akungba central) and 377 cps (P around AAUA Campus).

For the purpose of understanding the levels of the activity concentrations for ^{40}K, ^{238}U and ^{232}Th in these rocks in same unit of $Bqkg^{-1}$, the activity concentrations were computed from measured elemental concentrations and are shown in Table 2. The estimated activity concentrations of ^{40}K, ^{238}U and ^{232}Th for specific rocks in respective locations are as high as 2998.50 $Bqkg^{-1}$ (P of Akungba west to central), 239.59 $Bqkg^{-1}$ (P around Akungba north) and 380.42 $Bqkg^{-1}$(GGN around Akungba north), respectively. The estimated average of ^{40}K ranges from 169.02 (Ch) to 1652.64 $Bqkg^{-1}$ (P); both range of values are observed around the western to central Akungba. ^{238}U activity concentration ranges from 8.65 (P of Akungba west to central) to 84.60 $Bqkg^{-1}$ (P of Akungba east), while the ^{232}Th ranges from 17.59 (BGN of Akungba southeast) to 137.74 $Bqkg^{-1}$ (P of AAUA Campus). Low to high activity concentrations also correspond to their low and high elemental concentrations and vice versa. These observed variations serve as good indicator that some rocks (especially the BGN, GGN, BG and P) have activity concentrations far above the continental averages for rocks; hence, they are radioactive

in sections with high fractions of K-feldspar, plagioclase, biotite, and accessory and opaque minerals, and trace and rare earth elements than in other sections due to the variability in amounts of these rock-forming minerals and elements.

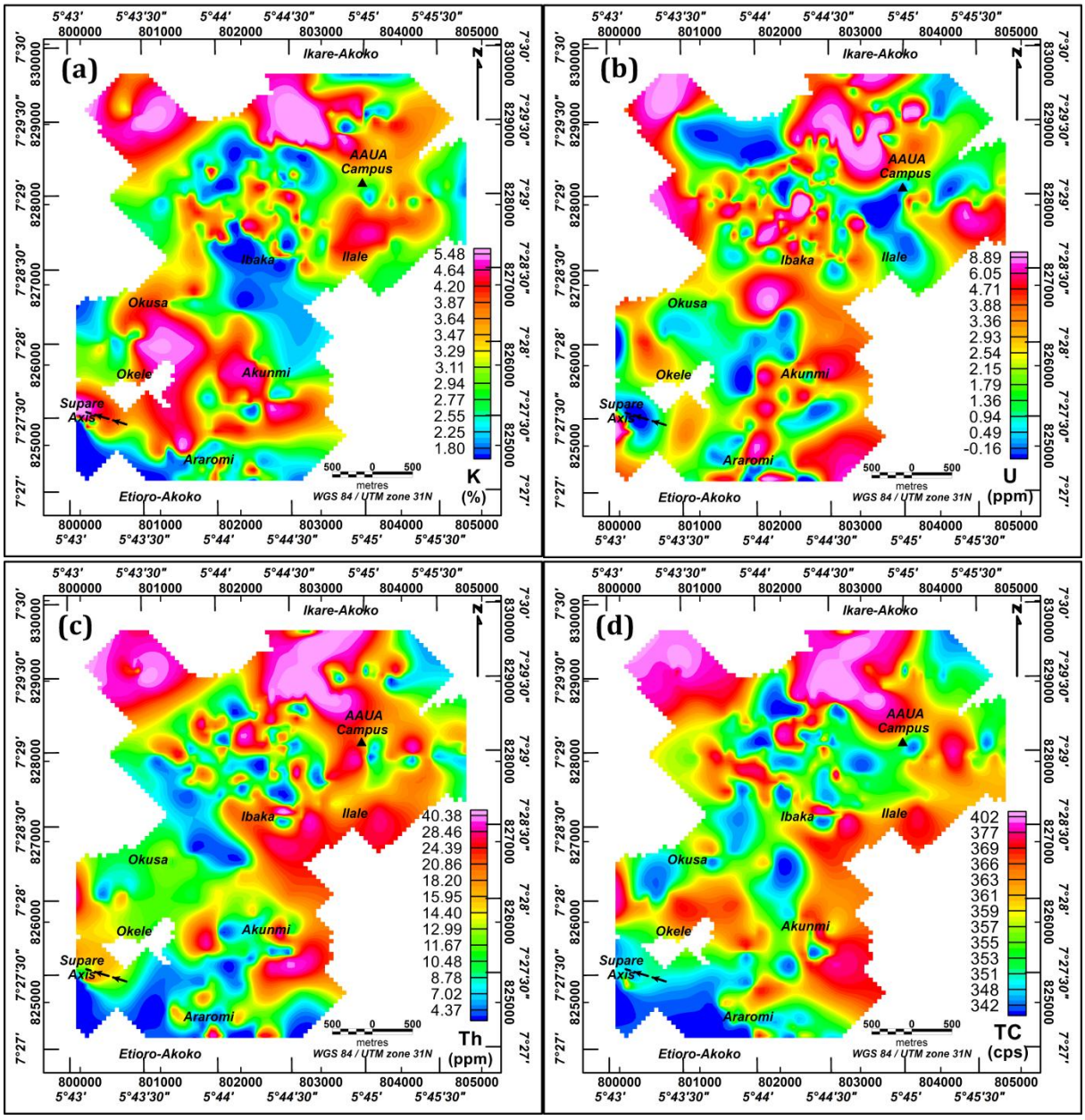

Fig. 3: Maps of: (a) potassium concentration, (b) uranium concentration, (c) thorium concentration, and (d) total count emission rate of Akungba-Akoko basement rocks.

Table 2: Distribution (range and mean) of elemental and activity concentrations, total counts and absorbed dose rates of Akungba-Akoko Basement Complex rocks at respective locations.

Location	Rock type	K (%)	eU (ppm)	eTh (ppm)	K ($Bqkg^{-1}$)	U ($Bqkg^{-1}$)	Th ($Bqkg^{-1}$)	TC (*cps*)	$\mathcal{D}$ ($nGy\,h^{-1}$)
		Elemental concentration			**Activity concentration**				
Akungba Southwest	P	1.80–6.04 (4.22)	BDL–6.50 (1.68)	BDL–28.60 (10.33)	563.40–1890.50 (1320.30)	BDL–80.28 (20.79)	BDL–116.12 (41.95)	336.0–365.40 (353.23)	60.90–114.60 (89.37)
	GGN	1.19–5.03 (3.12)	BDL–9.40 (2.18)	1.10–26.50 (12.10)	372.47–1574.39 (976.82)	BDL–116.09 (26.96)	4.47–107.59 (49.16)	319.5–367.50 (351.78)	39.70–123.30 (86.61)
	M	0.17–2.18 (1.46)	0.60–8.30 (4.65)	0.90–20.10 (6.40)	53.21–682.34 (455.42)	7.41–102.51 (57.43)	3.65–81.61 (25.98)	334.1–355.50 (345.57)	40.80–83.00 (61.75)
Akungba Southeast	P	2.56–5.16 (3.68)	BDL–4.80 (2.17)	1.60–14.30 (6.13)	816.93–1615.10 (1151.3)	BDL–59.28 (26.83)	6.50–58.06 (24.88)	333.7–364.90 (350.06)	57.90–105.50 (76.12)
	GGN	0.07–5.85 (3.03)	BDL–15.20 (2.73)	0.70–29.90 (12.28)	22.85–1831.10 (946.69)	BDL–187.72 (33.76)	2.84–121.39 (49.86)	328.8–370.00 (354.09)	43.60–146.20 (86.76)
	BGN	1.73–3.12 (2.52)	BDL–3.80 (2.27)	BDL–8.40 (4.33)	541.43–976.56 (788.76)	BDL–46.93 (27.99)	BDL–34.10 (17.59)	342.6–348.20 (346.13)	51.40–62.40 (56.97)
Akungba East	P	1.34–3.94 (2.62)	BDL–10.60 (6.85)	3.70–10.80 (5.72)	419.42–1233.20 (820.58)	BDL–130.91 (84.60)	15.02–43.85 (23.21)	348.8–356.70 (351.10)	66.00–97.40 (86.67)
	BG	0.46–6.76 (3.38)	BDL–13.60 (2.66)	BDL–63.40 (28.05)	143.98–2115.90 (1059.10)	BDL–167.96 (32.88)	BDL–257.40 (115.89)	327.2–408.90 (369.44)	41.20–299.70 (130.99)
	GGN	0.55–6.34 (3.04)	BDL–11.80 (2.59)	BDL–39.0 (14.14)	172.15–1984.42 (952.02)	BDL–145.73 (31.99)	BDL–158.34 (57.41)	333.1–379.10 (357.35)	41.20–155.0 (90.23)
Akungba West & Central	P	1.05–9.58 (5.28)	BDL–3.10 (0.70)	2.00–88.40 (23.51)	8.30–2998.50 (1652.64)	BDL–38.29 (8.65)	8.12–358.90 (95.47)	332.30–411.0 (369.30)	34.70–299.10 (131.93)
	Ch	BDL–1.86 (0.54)	BDL–4.90 (1.27)	BDL–20.40 (4.47)	BDL–582.18 (169.02)	BDL–60.52 (15.68)	BDL–82.82 (18.15)	319.8–354.50 (331.82)	1.80–75.30 (25.62)
	GGN	BDL-6.01 (3.06)	BDL-11.40 (3.16)	BDL–47.20 (14.58)	BDL–1881.10 (956.09)	BDL–140.79 (40.07)	BDL–191.63 (60.53)	329.2–414.70 (359.92)	16.10–212.30 (93.80)
Akungba North	P	0.97–6.88 (4.42)	BDL–19.40 (3.82)	0.90–42.40 (20.61)	303.61–2153.44 (1382.26)	BDL–239.59 (47.12)	3.65–172.14 (83.67)	331.7–413.80 (368.31)	59.40–267.70 (131.05)
	GGN	0.54–8.26 (3.53)	BDL–26.20 (3.70)	0.80–93.70 (21.69)	169.02–2585.40 (1124.50)	BDL–323.57 (45.66)	3.25–380.42 (88.07)	309.3–440.20 (369.02)	39.40–282.20 (120.63)
	BGN	0.13–5.09 (3.16)	BDL–16.40 (5.34)	BDL–30.30 (15.15)	40.69–1593.17 (989.22)	BDL–202.54 (65.90)	BDL–123.02 (61.49)	337.1–378.80 (360.76)	71.10–156.80 (110.34)
AAUA Campus	P	2.42–7.70 (5.07)	BDL–3.50 (1.43)	7.90–93.00 (33.93)	757.46–1708.68 (1585.35)	BDL–43.23 (17.60)	32.07–377.58 (137.74)	345.6–440.90 (377.60)	82.80–313.40 (159.53)
	BG	1.53–3.93 (2.63)	BDL–10.90 (2.75)	6.80–32.40 (17.31)	478.89–1230.10 (822.74)	BDL–134.62 (33.96)	27.61–131.54 (70.27)	335.4–370.50 (354.46)	57.50–127.10 (93.52)
	GGN	1.08–6.15 (3.18)	BDL–10.40 (2.24)	BDL–54.20 (15.15)	338.04–1924.95 (994.20)	BDL–128.44 (27.65)	BDL–220.22 (61.51)	336.2– 415.50 (357.47)	42.90–201.70 (93.32)

M – Migmatite, BGN – Biotite gneiss, GGN – Granite gneiss, Ch – Charnockite, BG – Biotite granite, P – Pegmatite, BDL – below detection limit. The values enclosed within the brackets indicate the estimated averages for each rock in specific locations in the study area.

Fig. 4 provides a pictorial view to better understand the variations of the activity concentrations of the radionuclides in each rock type. Generally, on average, the pegmatitic intrusives have the highest total activity concentrations, except at the eastern Akungba with slight decrease, while the charnockitic rocks depict the lowest activity concentrations compared with other rocks. The biotite gneisses and granite gneisses are second in activity concentrations to the pegmatites. The biotite granites around AAUA campus are next in line to these gneissic rocks. Hence, the increasing orders of total activity concentrations for the rocks are: M < GGN < P; BGN < GGN < P; P < GGN < BG; Ch < GGN < P; BGN < GGN < P; and BG < GGN < P for Akungba southwest, southeast, east, west – central, north and AAUA campus, respectively.

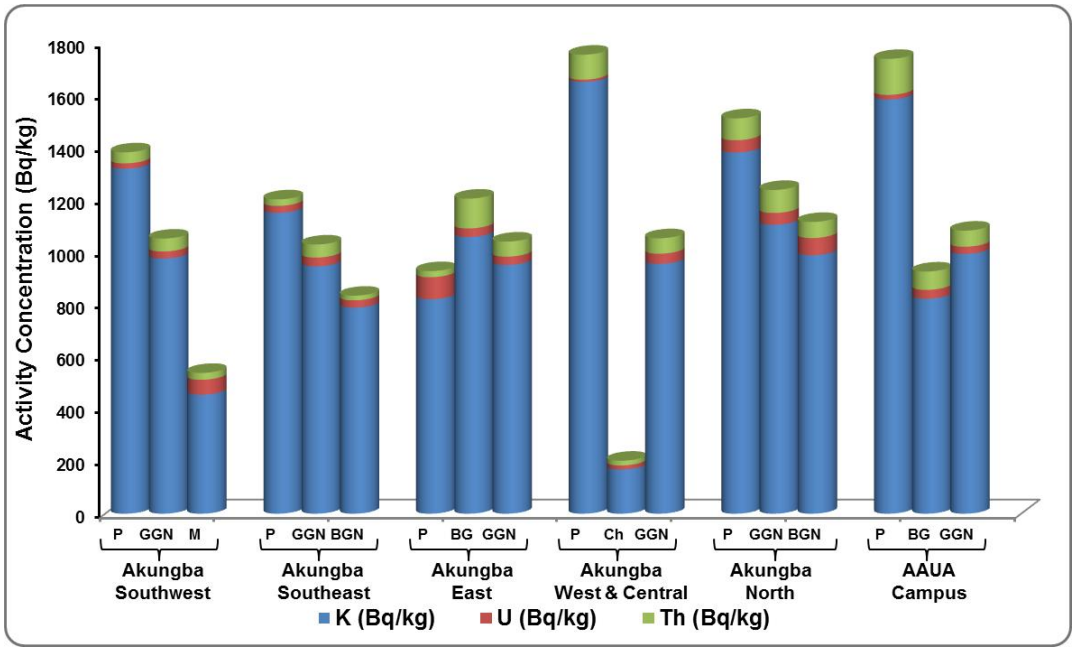

Fig. 4: Composite distribution plot of total activity concentrations of the rocks in specific locations within the study area.

The estimated average elemental and activity concentrations of ^{40}K, ^{238}U and ^{232}Th for each rock as presented in Table 3 show the exact average proportion of these radionuclides in each rock and their overall averages. This helps to relate their averages with the world averages for determining the levels of radionuclides increase in these rocks. The average elemental

concentrations of ^{40}K, ^{238}U and ^{232}Th for the rocks range from 0.54 – 4.24%, 1.27 – 4.85 ppm and 4.47 – 26.70 ppm. Their average activity concentrations range from 169.02 – 1327.89, 15.68 – 59.92 and 18.15 – 108.75 $Bqkg^{-1}$ for ^{40}K, ^{238}U and ^{232}Th, respectively. The overall mean values of 2.66%, 3.16 ppm and 13.98 ppm estimated for elemental concentrations of ^{40}K, ^{238}U and ^{232}Th are above the average crustal concentrations of 2.35%, 3 ppm and 12 ppm (IAEA 2003), and their environmental activity concentrations of 831.35, 39.1 and 56.77 $Bqkg^{-1}$ are also above the crustal standards of 420, 33, and 45 $Bqkg^{-1}$ (UNSCEAR, 2000), respectively. However, all concentration results obtained for charnockitic rocks are far below these standards as well as the eU and eTh concentrations of pegmatites and migmatites, respectively. The increase above these standards suggests the abundance of the NORMs in these rocks. The variations in estimated average activity concentrations are, therefore, displayed in Fig. 5. The increasing orders for average radionuclides in the rocks are: Ch < M < GGN < BGN < BG < P; Ch < P < BG < GGN < M < BGN; and Ch < M < BGN < GGN < P < BG, for ^{40}K, ^{238}U, and ^{232}Th, respectively.

Table 3: Average radionuclide concentrations, radium activity equivalent, dose rate and rate of radiogenic heat production for the rocks in the study area

Rock type	***N***	**K (%)**	**eU (ppm)**	**eTh (ppm)**	**K**	**U**	**Th**	Ra_{eq} **($Bqkg^{-1}$)**	$\mathcal{D}$ **($nGy\,h^{-1}$)**	**RHP (μWm^{-3})**
		Elemental concentration			**Activity concentration ($Bqkg^{-1}$)**					
P	45	4.24	2.59	16.09	1327.89	31.97	65.33	227.64	110.31	2.18
BG	80	3.30	2.70	26.79	1033.17	33.36	108.75	268.43	126.83	2.86
Ch	13	0.54	1.27	4.47	169.02	15.68	18.15	54.65	25.62	0.69
GGN	353	3.17	2.89	15.95	990.89	35.68	64.77	204.60	97.90	2.14
BGN	26	3.23	4.85	14.20	1011.70	59.92	57.65	220.26	105.48	2.53
M	6	1.46	4.65	6.40	455.42	57.43	25.98	129.65	61.75	1.78
Min		0.54	1.27	4.47	169.02	15.68	18.15	54.65	25.62	0.69
Max		4.24	4.85	26.70	1327.89	59.92	108.75	268.43	126.83	2.86
Mean		2.66	3.16	13.98	831.35	39.01	56.77	184.20	87.98	2.03

N is the number of measurement point

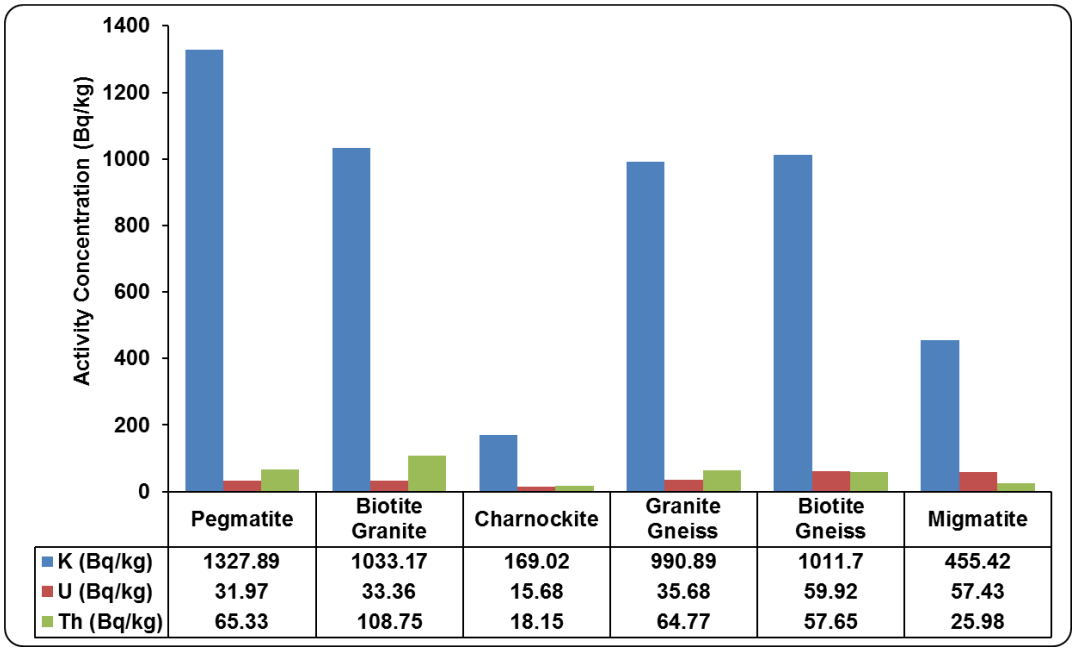

Fig. 5: Distribution plot of the exact activity concentration averages for Akungba-Akoko basement rocks.

5. Discussion

5.1 In situ gamma-ray spectrometry and radionuclides concentration in rocks

Geologically, based on the measured and estimated radionuclides, the generally observed low K-eU-eTh in the Akungba-Akoko charnockites compared to other rocks in the area is a function of their mineralogy, which is typical of charnockitic rocks (Smithson and Decker 1974; Killeen and Heier 1974, 1975), as shown in the modal and geochemical analyses presented in Table 4 by Ogunyele et al. (2019). Charnockites have the lowest average K-feldspar (18.30 vol.%), SiO_2 (58.64 wt.%), and opaque minerals (indicating amount of NORMs), but with biotite (8.40 vol.%) slightly higher than granite gneisses. Besides, the average Th content (12 ppm) is also the lowest. With exception of charnockites, other rocks within the normal intermediate to acid igneous protoliths differentiation series (BGN, GGN and BG), their eU and eTh generally increases progressively with acidity (Constable and Hubbard 1981). On the other hand, rocks with low eTh concentration (charnockites and migmatites are the most affected) may have been caused by the variability in mineral abundance, especially the accessory minerals (zircon and monazite) (Braun et al. 1993, 1998), or due to mobilization either during metamorphism or crystallization

processes (Youssef et al. 2017; Nisbet et al. 2019). When eU is also lowered in conjunction with eTh-concentrations below their continental averages (M, Ch and P; see Table 3) suggests the variability of the rock-forming minerals and trace elements and low eU-eTh concentration in the magma that formed the rocks (Constable and Hubbard 1981).

However, high concentration of the three radionuclides in pegmatites, granites and gneisses results from high fraction in K-feldspar, plagioclase feldspar, biotite and accessory minerals (Killeen and Heier 1974; Zhu and O'Nions 1999). The modal and geochemical results (Table 4) show that these rocks are rich in the minerals, but granite gneisses have much lower amount of biotite (7.25 vol.%) compared to BGN and BG with values of 10.15 and 20.15 vol.%, respectively. The average Th contents for these rocks range from 12.50 (BG) – 20 ppm (BGN); that of GGN is 17.33 ppm. Their average zirconium contents are very high, with values ranging from 82 – 124.5 ppm, and the yttrium (Y) is also very high with range between 24.33 ppm and 36.5 ppm (BG with the highest value) (see Table 4). The high biotite content of biotite granites (20.5 vol. %) in addition to other high NORMs compared to other rocks account for the observed very high radionuclides concentrations. The paraluminous nature of these rocks (Ogunyele et al. 2019) account for their enrichment in eTh than eU because high eTh is attributed to monazite, which is common accessory mineral found in paraluminous granitoids and occurs in some hydrothermal altered zones (Bea 1996; Zhu and O'Nions 1999). The modal and geochemical analyses for the Akungba basement complex rocks are in line with the radioactivity results; the average modal and geochemical results are in the order BG > BGN > GGN > Ch (Table 4) corresponding to their measured and estimated radioactivity concentrations (Table 2 and 3).

Table 4: Average modal and geochemical (major oxides and trace elements) compositions of Basement Complex rocks in Akungba-Akoko (Ogunyele et al. 2019).

	GGN	BGN	BG	Ch
Minerals (vol. %)				
Quartz	28.00	27.90	23.35	22.30
K-feldspar	25.95	22.50	20.15	18.30
Plagioclase	34.85	32.10	30.15	32.30
Biotite	7.25	10.15	20.15	8.40
Hornblende	3.30	6.80	4.15	6.00
Muscovite	1.70	1.30	1.50	5.30
Opaque	0.65	0.75	0.85	0.40
Pyroxene				7.70
Major oxides (wt.%)				
SiO_2	74.28	70.71	59.95	58.64
TiO_3	0.24	0.60	1.02	0.98
Al_2O_3	13.59	13.62	16.91	16.63
Fe_2O_3	3.59	4.46	6.67	6.70
MnO	0.04	0.05	0.14	0.21
MgO	0.27	0.88	2.97	2.85
CaO	2.64	3.60	5.80	7.02
Na_2O	1.85	1.84	0.76	0.76
K_2O	2.66	3.09	2.34	2.58
P_2O_5				0.01
Trace elements (ppm)				
Th	17.33	20.00	12.50	12.00
Y	24.33	27.00	36.50	34.67
Zr	82.00	96.00	124.5	115.0

5.2 Radioelement ratios, radioelement composite maps and F-parameter

To further substantiate the results of this study on rocks' radionuclides variability in the study area, the radioelement ratio and composite maps of the measured elemental radionuclides concentration were produced and analysed. The eU/eTh ratio values used for determining the abundance of eTh relative to eU are comprised between 0 and >1.38 %/ppm across the area studied (see Fig. 6a; Table 5). These values increase from pegmatites at AAUA Campus to pegmatites at Akungba west to central. A part of the sections occupied by granite gneisses also

shows high eU/eTh ratio (pink colour at the central and southern parts) including biotite granites at the extreme east (Fig. 6a). Some of the pegmatites depict low eU/eTh due to depletion of eTh (Constable and Hubbard 1981; Eleraki et al. 2017). Hence, the values of eU/eTh ratio higher than global ratio of 0.26 (Table 5) for the continental crust averages suggest the abundance of eTh than eU in the rocks (Chandrasekaran et al. 2014).

Due to the higher mobility of K than eTh, K/eTh ratio anomalies can provides clues on the variability and depletion of K-eTh contents arising from the nature and degree of alteration the rocks were subjected (Elkhateeb and Abdellatif 2018). The K/eTh ratio of the rocks in the study area ranges from <0.09 to >0.87 %/ppm (Fig. 6b). The NW-SE trending low K/eTh marks the contact of GGN and BG and suggests the interaction of BG magma with the already formed GGN, probably through assimilation process, or weathered rock unit. The exact average K/eTh values for each rock range from 0.12 (Ch) – 0.6 %/ppm (P of Akungba southeast) (see Table 5). BG and P (AAUA Campus), GGN (Akungba north), Ch (Akungba west-central) and BG (Akungba east) are the set of rocks within the specified constant range of 0.17 – 0.2 %/ppm as suggested by Hoover et al. (1992) as the stable K/eTh ratio range for most rocks. The estimated overall average K/eTh for the rocks is 0.29 %/ppm (Table 5, reddish colour scale and above in Fig. 6b) and is above this range of values. Taking into cognizant of this overall average and the estimated low K/eTh ratio values below and within the proposed range suggests the variability in K-eTh contents in the rocks, especially for sections characterised by high K concentration relative to eTh (Portnov 1987; Elkhateeb and Abdellatif 2018).

The eU/K ratio, on the other hand, determines relatively enriched uranium content in the rocks. Its spatial values across the study area are comprised between 0 and 3.25 %/ppm (Fig. 6c; Table 5). In this case, the high and low ratio values are depicted by pegmatites at Akungba west-central (expected to have highest K) and migmatite at Akungba southwest, respectively. Comparing the results of eU/eTh with eU/K, migmatite has a value of 0.73 eU/eTh ratio (Table 5) suggesting the mobilization of eU which in turns alters the eU/eTh ratio (Eleraki et al. 2017). These anomalies are also observed in granite gneisses at the central to southeastern axis.

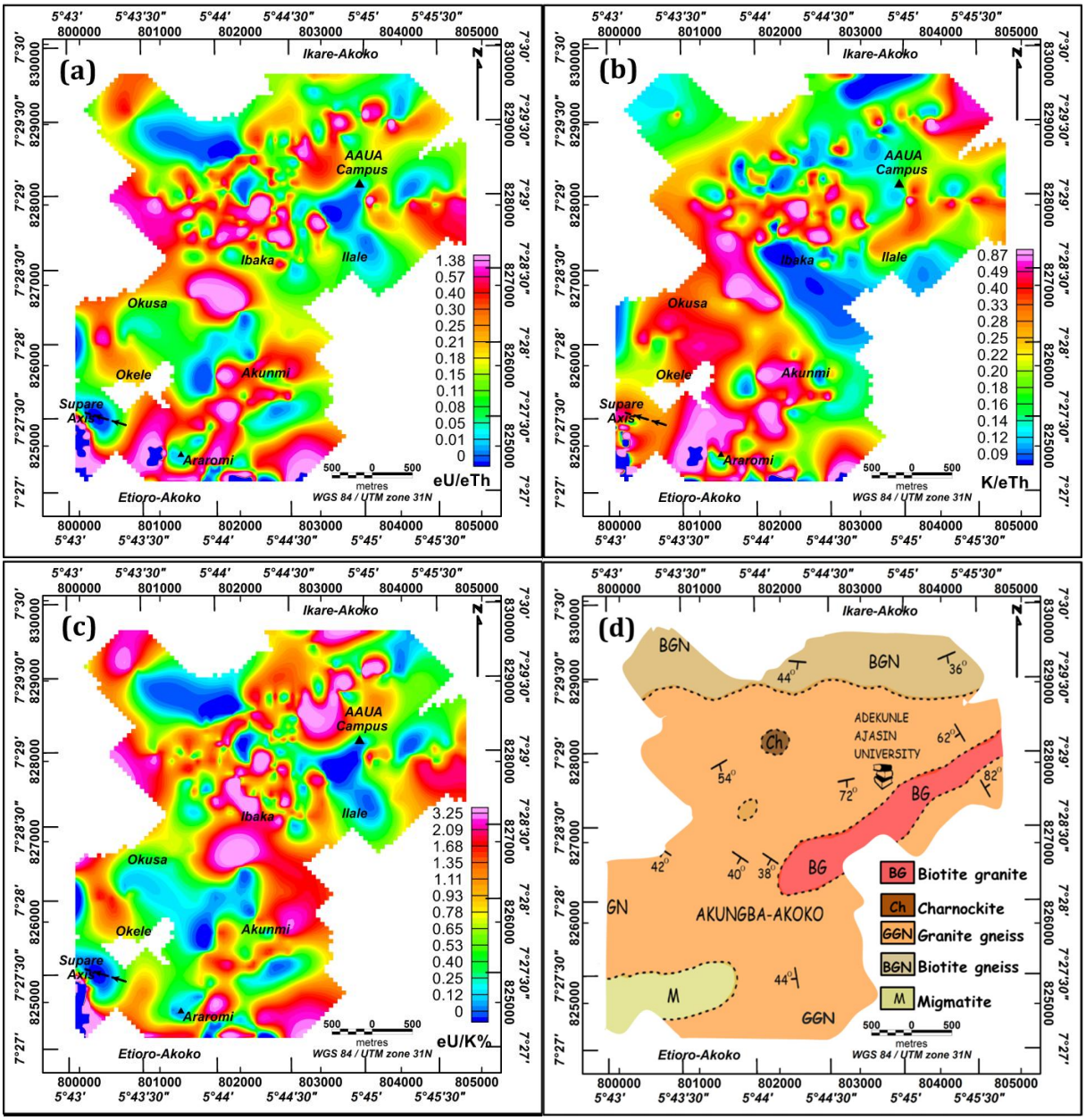

Fig. 6: Maps of: (a) eU/eTh ratio, (b) K/eTh ratio, (c) eU/K ratio, and (d) sectionalized geological map of Akungba-Akoko. The sectionalized geological map is placed with the other map for easy identification and detailed understanding of the radioelements variation across the lithological units.

Table 5: Radioelement ratios and F-parameter of Efimov of Akungba-Akoko Basement Complex rocks (parameters were estimated using K, eU and eTh in %, ppm and ppm, respectively)

Location	Rock Type	eU/eTh	K/eTh	eU/K	F-parameter of Efimov K*(eU/eTh)
Akungba Southwest	P	0.16	0.41	0.40	0.67
	GGN	0.18	0.26	0.70	0.56
	M	0.73	0.23	3.19	1.06
Akungba Southeast	P	0.36	0.60	0.59	1.30
	GGN	0.22	0.25	0.90	0.67
	BGN	0.52	0.58	0.90	1.32
Akungba East	P	1.20	0.46	2.62	3.14
	BG	0.10	0.12	0.79	0.32
	GGN	0.18	0.22	0.85	0.56
Akungba West & Central	P	0.03	0.23	0.13	0.16
	Ch	0.28	0.12	2.35	0.15
	GGN	0.22	0.21	1.03	0.66
Akungba North	P	0.19	0.22	0.86	0.82
	GGN	0.17	0.16	1.05	0.60
	BGN	0.35	0.21	1.69	1.11
AAUA Campus	P	0.04	0.15	0.28	0.21
	BG	0.16	0.15	1.05	0.42
	GGN	0.15	0.21	0.70	0.47
Mean		**0.29**	**0.27**	**0.87**	

The three-radioelement composite map (Fig. 7a) and radioelement composite maps (Fig. 7b-c) of the Akungba-Akoko Basement Complex rocks show the abundance proportion of measured K%, eU and eTh and the abundance of one radioelement over the other two, respectively. The ternary diagram used assumes that the summation of these three radioelements is 1.0 or 100% (Erbek and Dolmaz, 2018). The three-radioelement and their composite maps are widely used for revealing the surface radioelement distribution, discriminating of widespread lithologies, and mapping of rocks' contacts (Youssef and Elkhodary 2013). These are analysed by using the ternary image colour zoning in relation to viable rocks' mineralogy, especially those that give rise to K, eU and eTh (Dickson and Scott, 1997; Abd El Nabi, 2012). The colour zoning of red, green and blue were used for K, eTh and eU, respectively, for the three-radioelement composite map. The blue colour tends to reduce the most reduced signal-to-noise ratio of uranium channel.

The white and black colour zones denote high and low concentrations of the three radioelements, respectively, in the three-radioelement composite map. In the potassium composite map (Fig. 7b) it combines K (in red) with the two ratios K/eTh (in green) and K/eU (in blue), uranium composite map (Fig. 7c) combines eU (in red) with the two ratios eU/eTh (in green) and eU/K (in blue), and thorium composite map (Fig. 7d) combines eTh (in red) with the two ratios eTh/eU (in green) and eTh/K (in blue).

The three-radioelement composite map (Fig. 7a) shows high K% and sparse pockets of high eTh and eU concentrations within and around the southern part between longitudes 800000 and 803200 mE and latitudes 825200 and 827000 mN. The NW-SE eU trend interspersed by varying K-eU-eTh concentrations stretches from the southeastern where the biotite granite terminates to northwestern part where the biotite gneisses outcrop. This feature separates the southern signatures from that of the central part with high eU concentration and sparse concentrations of K% and eTh. The yellowish to greyish, blackish to whitish, and light greenish colourations occupying the northern flank suggest almost equal eTh and K concentrations, low to high enriched K-eU-eTh concentrations, and gradually reducing concentration strength of K, respectively. AAUA Campus also depicts same characteristic signatures, but with more abundance of eTh than eU.

In Fig 7b-d, the anomalous zones depict bright colours. Fig. 7b shows varying K% signatures from the central to the northern axis in rocks located within, while the southern half depicts consistently moderate to high K. The NW-SE trending signature identified in Fig. 6b demarcates these two sections of the map and itself being low in K. Fig 7c provides additional information on high eU compared to the two other radioelements. High eU zones depict bright white colour, mostly seen in the granite gneisses at the central and a part of the northern biotite gneisses, while the dark coloured areas characterise rocks with low eU concentration (Youssef and Elkhodary 2013), probably due to eU migration which is seen as the dominant event in the rocks. Interestingly, when compared with Fig. 7d, the eTh shows two major contrasting concentration levels in the rocks; the high eTh attributed to half section from the central to the northern axis and the other half from central to the southern part with varying concentrations dominated by low eTh scattered across the rock units.

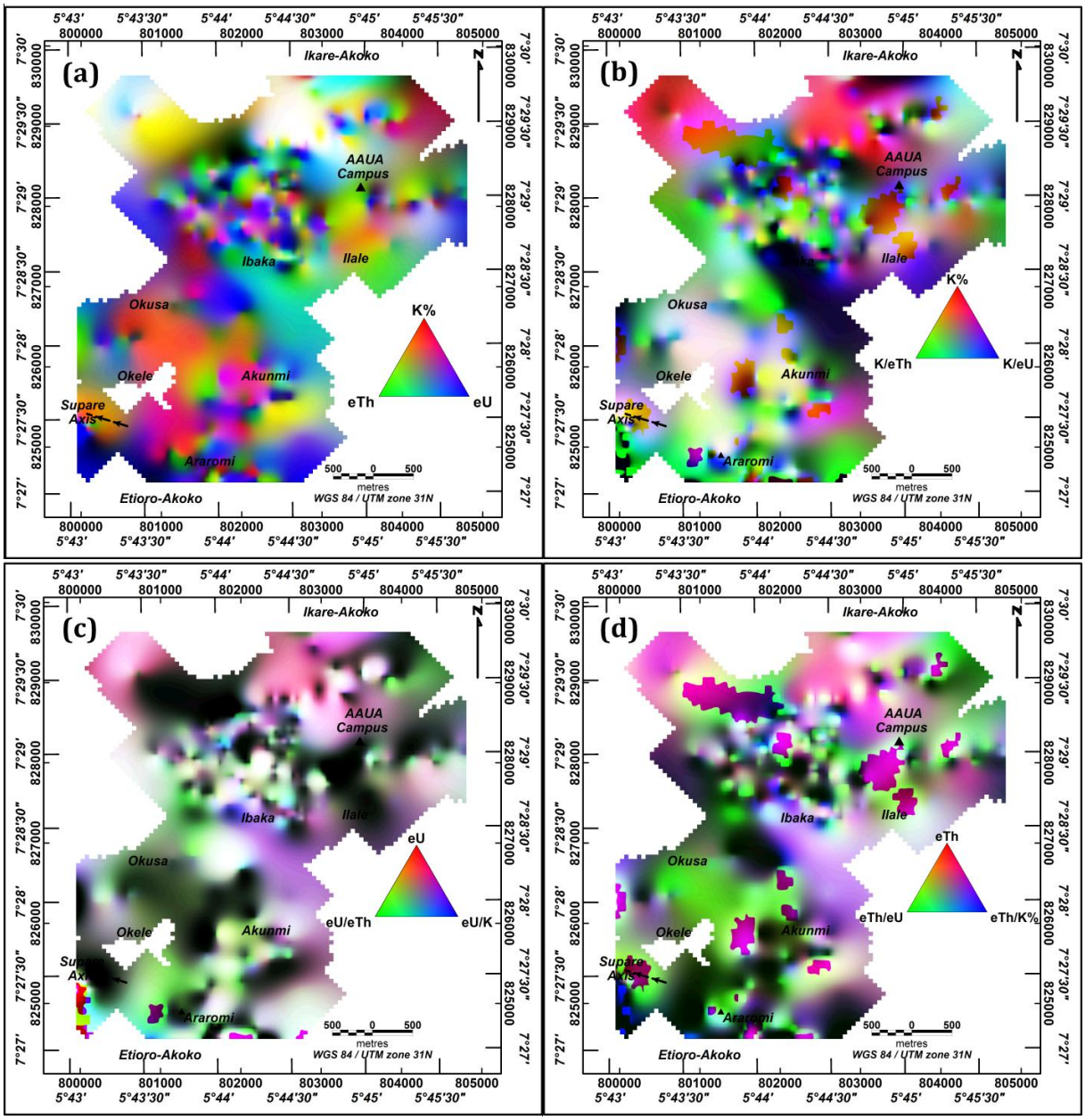

Fig. 7: Maps of: (a) three-radioelement composite, (b) potassium composite, (c) uranium composite, and (d) thorium composite of Akungba-Akoko basement rocks.

The F-parameter of Efimov approach (Efimov 1978) is denoted by K*(eU/eTh) and expressed as concentration of potassium abundance multiplied by the ratio of eU and eTh. This parameter can also be expressed as ratio of uranium abundance and eTh/K denoted as eU/(eTh/K) or as ratio of potassium abundance and Th/U donated as K/(eTh/eU). This is an important factor for determining the alteration index of rocks. The F-parameter values for unaltered rocks are not

greater than 1.2 – 1.3, while that of the altered rocks are within 2 – 5 and can as well be greater than 10 (Gnojek and Prichystal 1985; Abd El Nabi 2012). The estimated F-parameter values for Akungba-Akoko Basement Complex rocks range from 0.15 – 3.14 (see Table 5). The biotite gneissic and pegmatitic rocks around the southeastern and eastern parts have F-parameter values of 1.32 and 3.14, respectively, which are above the values for unaltered rocks. This suggests evidence of alterations from metamorphism and crystallization processes (Abd El-Naby and Saleh 2003).

5.3 Radiological hazard parameters

5.3.1 Radiogenic heat production

Rocks producing radiogenic heat provide insights into lithospheric heat flux and proper understanding of processes related to the thermal evolution of the earth as well as potential sources of geothermal energy (Sabra et al. 2019). The main mechanism of RHP within the earth's crust is the decay of four naturally occurring isotopes (^{40}K, ^{235}U, ^{238}U and ^{232}Th) which are the products of radioactive heat-producing elements: K, eU and eTh (Schmucker 1969). The RHP of these elements varies: 1% K_2O produces about 0.074 $\mu W m^{-3}$, almost equal to 1 ppm Th with RHP of about 0.072 $\mu W m^{-3}$, but 1 ppm of eU produces about 0.264 $\mu W m^{-3}$, nearly four times greater than that of 1 ppm Th or 1% K_2O. The higher RHP rate of eU is due to its two radioactive isotopes (^{235}U and ^{238}U), and the faster decaying of these isotopes than ^{232}Th (Bea 2012). The RHP intensity in crustal formations depends not only on the average concentration of these radioactive elements or their isotopes, but also on the vertical position of the rich sections containing radioactive heat-producing elements in the crustal formations. Heat-producing elements are not accumulated in mantle minerals, but are preferentially accumulated into continental crust (Rudnick and Fountain 1995). Therefore, RHP varies over geological time due to two different effects, which include enrichment caused by progressive extraction from the mantle and depletion caused by radioactive decay. The radioactive heat-producing elements concentration decrease with depth, and also they decrease progressively with increase in metamorphic grade (Oxburg 1980; Bea 2012).

The RHP for Akungba Basement Complex rocks (Fig. 8) are categorised into three based on their heat production rates. Low RHP rates (<1.21 $\mu W m^{-3}$) are attributed to the southern edges,

western to central parts and NNE rim of the area, which are the lowest radionuclides enriched zones (i.e. migmatites, and a large part of the southern and west/central granite gneisses and charnockites). The moderate RHP rates (1.21 – 2.50 μWm^{-3}) separate the low and high values into either trend-like forms or oblong to circular closures. High RHP rates (2.51 – 5.20 μWm^{-3}) are indicative of zones with high concentrations of the three radionuclides. The obtained average of RHP for specific rocks in the area range from 0.69 (Ch) – 2.86 μWm^{-3} (BG) with overall mean value of 2.03 μWm^{-3} (see Table 3). The observed high rates of RHP typically from pegmatites, biotite gneisses at northern part, biotite granites at the east to central and the southeastern rim granite gneisses, suggests that RHP increases as a function of increasing felsic and alkali contents as well as Fe content in plutonic (Hasterok and Webb 2017) (see Table 4, Ogunyele et al. 2019). In addition, the heat production of metamorphic rocks generally depends on the radioelement contents of their protoliths, modified by metamorphic processes (Wollenberg and Smith 1987). The RHP average of the studied rocks (2.03 μWm^{-3}) is above the crustal average range of 0.8 – 1.2 μWm^{-3} (Bea 2012; Youssef 2016); suggesting significant contribution to the heat flux in the studied area.

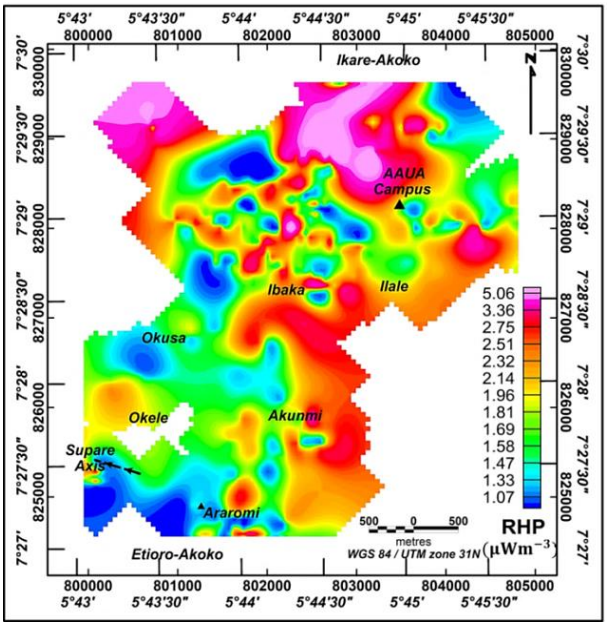

Fig. 8: Rate of radiogenic heat production map of the study area.

5.3.2 Radium equivalent activity and annual absorbed dose rate

The radium equivalent (Ra_{eq}) activity of the Akungba Basement Complex rocks provides insight on the level of potential risks of non-uniformity radiation from crustal rocks containing concentrations of ^{40}K, ^{238}U and ^{232}Th. In the activity map (Fig. 9), the southern rim, central and NNE edge of the area show very low radium equivalent below 159 $Bqkg^{-1}$. Moderate values of 160 – 210 $Bqkg^{-1}$ are distributed within the southern to northeastern part while the highest values (>210 $Bqkg^{-1}$) are observed around the southeastern through eastern rim to the northern and NNW flank of the area, including the trend-like patterns within the central part. High radium activity values are associated with areas with high radionuclides concentration. On the contrary, the estimated average Ra_{eq} activity for each rock type are shown in Table 3, and the values range from 54.65 (Ch) – 268.43 $Bqkg^{-1}$ (BG) with overall mean of 184.20 $Bqkg^{-1}$. This estimated mean is found below the world standard average of 370 $Bqkg^{-1}$ (UNSCEAR 2000) for crustal rocks; thus, suggesting that the emission from the radionuclides is negligible. However, the very high values above this permissible standard in some sections (Fig. 9) suggest elevated radium activity which may be injurious to human health if the affected rocks are abundantly used for constructions.

The isodose map depicting the annual absorbed dose rates in Akungba Basement Complex rocks (Fig. 10) were categorized based on the degree of radiological hazard risks; very low values (<60 $nGy\ h^{-1}$) correspond to the average world permissible limit (UNSCEAR 2000), low to moderate (60 – 120 $nGy\ h^{-1}$) and high values (>120 $nGy\ h^{-1}$). Sections of the map with high and low absorbed dose rate depict similar trend to the radium equivalent activity map (Fig. 9). The results of the measured dose rates for each rock in the specific locations range from 1.80 (Ch) – 313.40 $nGy\ h^{-1}$ (P around the AAUA Campus) (see Table 2). High average dose rates with values of 130.99 $nGy\ h^{-1}$ and 159.53 $nGy\ h^{-1}$ mainly in biotite granites around the eastern section and in pegmatites at the central to northern parts of the study area, respectively, are also observed. Table 3, on the other hand, presents the estimated averages for all the rocks with values ranging from 25.62 – 126.83 $nGy\ h^{-1}$. However, the estimated overall mean absorbed dose rate of 87.98 $nGy\ h^{-1}$ (Table 3) for the rocks is above the world permissible limit, but within the permissible range of 28 – 120 $nGy\ h^{-1}$ (UNSCEAR 2002). The observed average dose rate being found to

fall within the permissible range affirms the result of the radium equivalent activity, but also suggests the same precautionary measures.

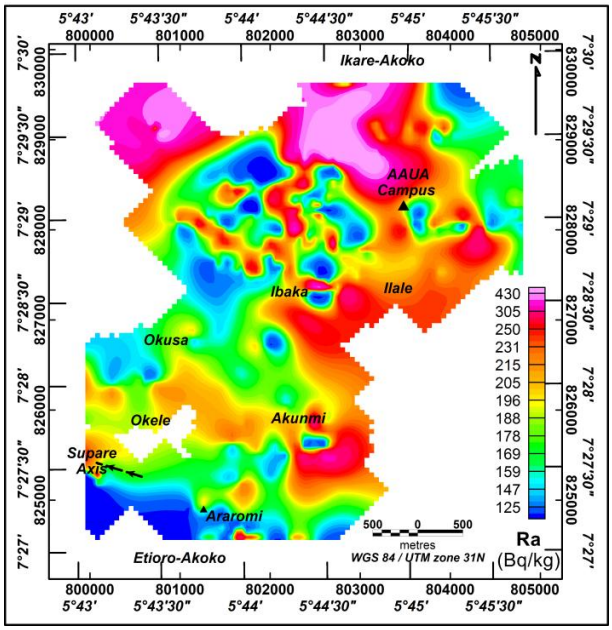

Fig. 9: Radium equivalent activity map.

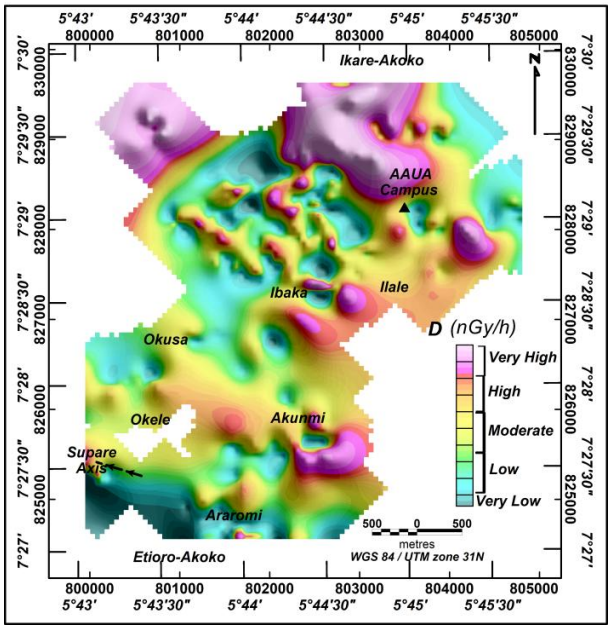

Fig. 10: Isodose map of the study area.

5.3.3 Correlation analysis (measured annual absorbed dose rate against radionuclides activity)

The correlation plots of the absorbed dose rates against activity concentrations (^{40}K, ^{238}U and ^{232}Th) and Ra_{eq} activity for Akungba Basement complex rocks at specific locations are shown in Fig. 11a-d. The plots show significantly strong positive correlations of 0.7163 and 0.8463 for the plots of absorbed dose rates against K and eTh, respectively (Fig. 11a and b). This suggests significant contribution from high concentration of these radionuclides to the observed increase in absorbed dose rate. However, the weak positive correlation of 0.0005 for absorbed dose rate against eU concentration (Fig. 11c) suggests low contribution of the eU compared to other radionuclides. Fig. 11d, on the other hand, shows a very strong positive correlation (0.9972), which is approximately unity, suggesting significant contribution of all radionuclides at their uniform activity concentration levels to the absorbed dose rate. Geologically, the observed strong positive correlation is an evidence of abundant radionuclides with major contribution from high fraction in rock-forming minerals – K-feldspar, plagioclase and biotite, and accessory minerals and trace elements. Conversely, the weak positive correlation of eU is an indication to

highly leached eU from the rocks and low eU concentration of the magma forming these rocks, which are the potential cause for this almost zero positive correlation compared to its counterpart (eTh).

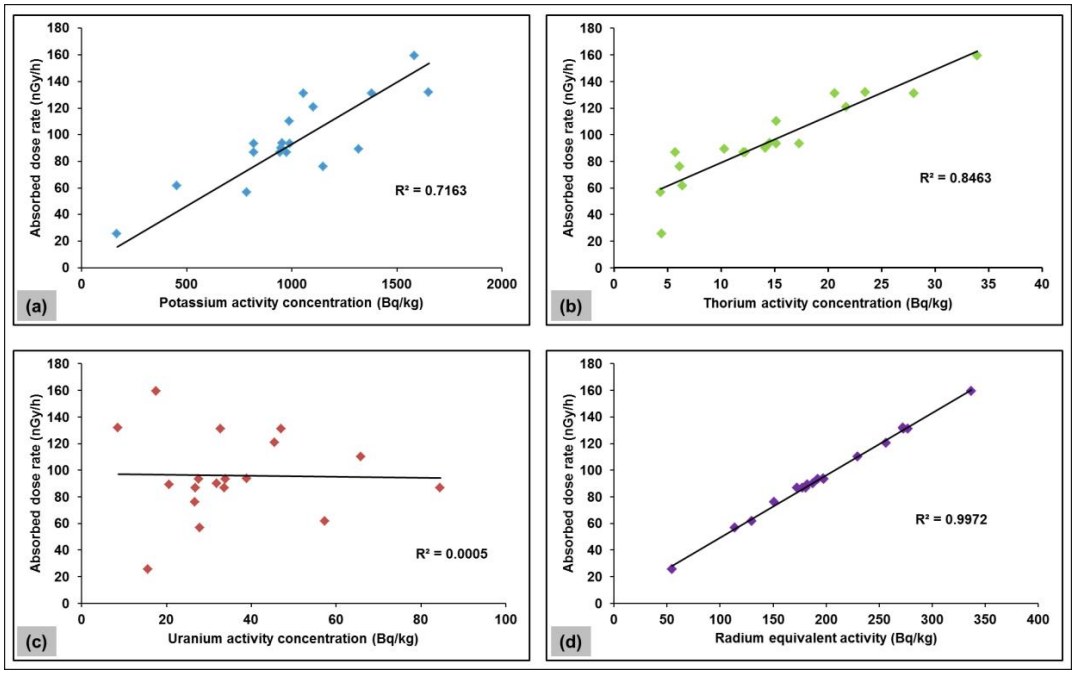

Fig. 11: Correlation plots of measured absorbed dose rate against; potassium activity concentration (a), thorium activity concentration (b), uranium activity concentration (c) and, radium equivalent activity (d).

5.3.4 Annual effective dose, radiological hazard indices, gamma activity index, activity utilization index, annual gonad dose equivalent and excess life cancer risk

The results of $AEDE_{out}$ and $AEDE_{in}$, RH_{ex} and RH_{in} indices, AC_{γ} and AUI estimated for Akungba-Akoko Basement Complex rocks to determine if the environment is radiologically safe or not for inhabitants are shown in Table 6. The $AEDE_{out}$ and $AEDE_{in}$ for the study area range from 0.031 – 0.156 $mSv\ y^{-1}$ and 0.126 – 0.622 $mSv\ y^{-1}$, respectively, with mean values of 0.108 and 0.432 $mSv\ y^{-1}$. The estimated mean values of AEDE for both outdoor and indoor are above the average worldwide limits of 0.07 $mSv\ y^{-1}$ and 0.41 $mSv\ y^{-1}$ respectively, except charnockites (UNSCEAR 2000), but both estimated average are far below the world upper limit of 1 $mSv\ y^{-1}$ (ICRP 1977). The RH_{ex} and RH_{in} indices ranging from 0.148 – 0.725 and 0.190 – 0.815 with mean values of 0.498 and 0.603, respectively, are lower than the recommended

standard of unity (1) (Ramasamy et al. 2009). Estimated AC_γ to determine the effects of gamma radiations on humans ranges from 0.199 – 0.999 with mean 0.691 (Table 6), and are lesser than $AC_\gamma \leq 2$ corresponding to gamma activity lower than $0.3\, mSv\, y^{-1}$and are far lower than the upper recommended limit of $1\, mSv\, y^{-1}$ (EC 1999). The AUI for determining the danger associated with gamma doses in air from radiations of ^{40}K, ^{238}U and ^{232}Th in the rocks ranging from 0.378 – 1.707 with mean 1.114, are also below the $AUI = 2$ corresponding to annual effective dose less than $0.3\, mSv\, y^{-1}$ (El-Gamal et al. 2007). Hence, both parameters suggest negligible gamma radiation effect. The estimated AGDE and ELCR range from 177.355 – 882.084 $\mu Sv\, y^{-1}$ and $0.440 * 10^{-3}$ – $2.178 * 10^{-3}$, with averages of 618.874 $\mu Sv\, y^{-1}$ and $1.511 * 10^{-3}$, respectively. These values are higher than the world permissible limits of 300 $\mu Sv\, y^{-1}$ (Xinwei et al. 2006) and $0.29 * 10^{-3}$ (Tufail *et al*., 2007) for AGDE and ELCR, respectively.

Table 6: Estimated radiological hazard parameters for Akungba-Akoko basement rocks.

Rock type	***N***	**AEDE ($mSv\, y^{-1}$)**		**RH_{ex}**	**RH_{in}**	**AC_γ**	**AUI**	**AGDE ($\mu Sv\, y^{-1}$)**	**ELCR (10^{-3})**
		Outdoor	**Indoor**						
P	45	0.135	0.541	0.615	0.701	0.876	1.194	788.830	1.894
BG	80	0.156	0.622	0.725	0.815	0.999	1.707	882.084	2.178
Ch	13	0.031	0.126	0.148	0.190	0.199	0.378	177.355	0.440
GGN	353	0.120	0.480	0.553	0.649	0.773	1.193	692.092	1.681
BGN	26	0.129	0.517	0.595	0.757	0.825	1.333	743.816	1.811
M	6	0.076	0.303	0.350	0.505	0.473	0.882	429.064	1.060
Min		0.031	0.126	0.148	0.190	0.199	0.378	177.355	0.440
Max		0.156	0.622	0.725	0.815	0.999	1.707	882.084	2.178
Mean		0.108	0.432	0.498	0.603	0.691	1.114	618.874	1.511

The estimated radiological parameters for the study area increase in the order: Ch < M < GGN < BGN < P < BG (see Table 6); charnockite and biotite granite having the minimum and maximum values respectively. In spite of the high concentration of the three radionuclides in rocks, all the

estimated radiological parameters (AEDEs, RHs, AC_γ and AUI) are generally far below the world upper limit of 1 $mSv\ y^{-1}$ (Fig. 12a) and standard limit of unity (Fig. 12b) recommended by UNSCEAR (2000) for a radiologically safe environment. However, increase above the world permissible limits for AGDE and ELCR does not mean that the associated health threats of gonad diseases and cancer are expected to occur in people living in the study area. This increase is a pointer for humans to reduce high applications of the rocks (pegmatite and biotite-rich rocks) with high radionuclides concentration. Since there are no reports of cases of life threatening radiological illness coupled with the results of the radiological parameters far below the recommended standards, suggest radiologically safe environment for the inhabitants for now.

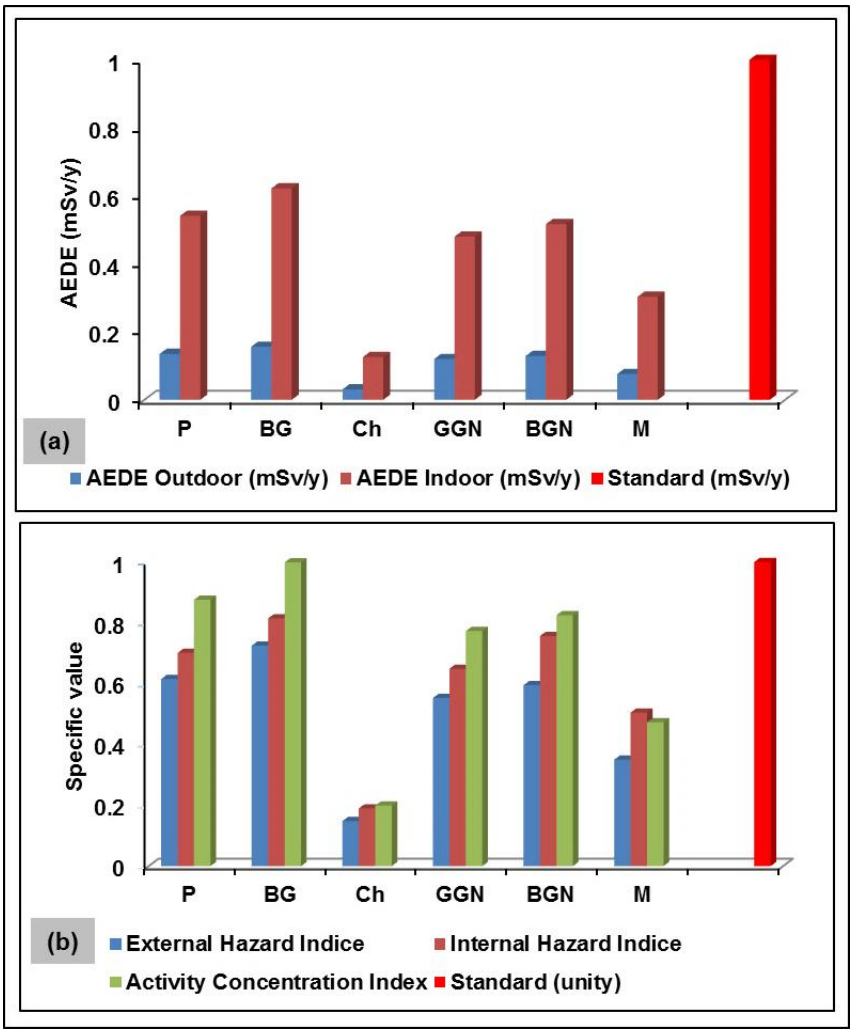

Fig. 12: Distribution plots of (a) $AEDE_{out}$ and $AEDE_{in}$, and (b) RH_{ex} and RH_{in} indices and AC_γ, as recommended radiological hazard parameters to determine the significance of gamma

radiations in Akungba-Akoko basement rocks. *These radiological parameters are all below the standard limits of 1 $mSv\,y^{-1}$ and unity; thus, radiological threat from gamma radiations is insignificant.*

The results of the activity concentrations and some of the radiological hazard parameters from this study were compared with results obtained from studies conducted in Nigeria and other countries and world permissible standards as shown in Table 7. On critical examination, the reported values of radionuclides in topsoil samples from Oka-Akoko, Ondo State, Nigeria, are far too lower than those reported in this study. This implies that the use of topsoils for radionuclides characterisation and environmental radiation risk assessment are somewhat ineffective, as soils do not contain the bulk radionuclides after being eroded from their sourced areas. The radioactivity results of granite gneisses of Akunu-Akoko and Ayere in Nigeria show high values of ^{40}K of approximately 202 $Bqkg^{-1}$; these values are, however, lower than the estimated averages for Akungba-Akoko Basement Complex rocks (see Table 6). Their ^{238}U and ^{232}Th values, on the other hand, are closer to the respective averages computed for this present study. This probably implies that the gneissic rocks in Akunu-Akoko and Ayere have similar radiochemistry and may have undergone similar geological processes. Akungba-Akoko Basement Complex rocks have high K compared to reported averages in other parts of the world, except Tamil Nadu rocks in India. This comparison provides better understanding on the need to utilize *in situ* rocks' radionuclides assessment to derive information on radiogeochemistry and previously operated geological processes.

Table 7: Comparison of GRS results of Akungba-Akoko Basement Complex rocks with averages in different parts of the world.

Country	^{40}K	^{238}U	^{232}Th	$AEDE_{in}$	$\mathcal{D}$	ELCR	Reference
	Activity concentration ($Bqkg^{-1}$)			($mSv\ y^{-1}$)	($nGy\ h^{-1}$)	(10^{-3})	
China	580	40	49				Tan et al. 1991
Hong Kong	530	59	95		87		UNSCEAR 2000
Malaysia					92	2.5	UNSCEAR 2000
Pankistan				0.49	70	0.54	Rafique et al. 2014
Mulga City, Turkey	340	28.5	27		53		Erbek and Dolmaz 2018
Tamilnadu, India	1146.88	19.16	48.56		40 – 135	0.70	Chandrasekaran et al. 2014
United States	370	40	35		47		UNSCEAR 2000
Oka-Akoko, Nigeria (Topsoil)	173	4.84	4.84		13		Ajayi and Ajayi 1999
Akunu and Ayere, Nigeria	629.28	38.58	49.96	0.364	73	1.273	Akingboye and Ademila 2019
World	420	33	45	1.0	60	0.29	UNSCEAR 2000; Tufail et al. 2007
Akungba-Akoko, Nigeria	831.35	39.01	56.77	0.432	87.98	1.51	Present Study

6. Conclusions

The results of ground GRS of Akungba-Akoko Basement Complex rocks, southwestern Nigeria, have proven the effectiveness of this method in determining spatial distribution of rocks' radionuclides concentration, radiogenic heat production rate, and environmental radiation risk associated with ^{40}K, ^{238}U and ^{232}Th to humans.

The overall average elemental and activity concentrations of Akungba-Akoko Basement Complex rocks are 2.66%, 3.16 ppm and 13.98 ppm, and 831.35, 39.01 and 56.77 $Bqkg^{-1}$ for ^{40}K, ^{238}U and ^{232}Th, respectively. This increase above average crustal abundance suggests

radionuclides abundance in the order: Ch < M < GGN < BGN < BG < P, Ch < P < BG < GGN < M < BGN, and Ch < M < BGN < GGN < P < BG in K, eU, and eTh, respectively. This is as result of high fraction of K-feldspar, plagioclase feldspar, biotite and accessory minerals – zircon, monazite, etc., and rare earth elements. Whereas, the observed low radionuclides concentration in migmatites and charnockites than in other rocks is caused by radionuclides variability of the rock-forming minerals, and trace and rare earth elements and their differentiation arising from metamorphism and crystallization as suggested by K/eTh ratio and F-parameter of Efimov.

The observed RHP rates for the studied rocks of 0.69 – 5.20 μWm^{-3} with average of 2.03 μWm^{-3} above the world crustal RHP average may have contributed to the increase in heat flux experienced in the study area. However, the charnockitic rocks have values below the world crustal average. The radiological hazard parameters due to gamma radiations from the rocks, which include average Ra_{eq} activity of 184.20 $Bqkg^{-1}$ is below the world limit of 370 $Bqkg^{-1}$ and the average absorbed doses of 87.98 $nGy\ h^{-1}$ is above the world permissible mean of 60 $nGy\ h^{-1}$, but still within the permissible range of 28 – 120 $nGy\ h^{-1}$. Other estimated averages for radiological parameters – $AEDE_{out}$ and $AEDE_{in}$, RH_{ex} and RH_{in} indices, AC_{γ} and AUI for Akungba-Akoko are far below the recommended upper world permissible limit of 1 $mSv\ y^{-1}$; thus, suggesting radiologically safe environment. These estimated radiological parameters for the rocks increase in the order Ch < M < GGN < BGN < P < BG. However, the estimated AGDE and ELCR with averages of 618.874 $\mu Sv\ y^{-1}$ and $1.511 * 10^{-3}$ which are above the world permissible limits of 300 $\mu Sv\ y^{-1}$ and $0.29 * 10^{-3}$, respectively, are pointers for drastic reduction in high applications of pegmatitic and biotite-rich rocks for construction works or any other application. The regular monitoring of the radiological hazard level of the study area is advised.

Acknowledgements

The authors greatly appreciate the Editor-in-Chief (James Wood LaMoreaux, PhD) and the two anonymous reviewers for their insightful comments, which contributed enormously to the quality of this work and increased its readability.

Funding

This research did not receive any specific grant from funding agencies in the public, commercial, or not-for-profit sectors.

Declaration of competing interest

The authors declare that they have no known competing financial interests or personal relationships that could have appeared to influence the work reported in this paper.

References

Abd El Nabi SH (2012) An Analysis of Airborne Gamma Ray Spectrometric Data of Gabal Umm Naggat Granitic Pluton, Central Eastern Desert, Egypt. *JAKU: Earth Sci* 23(2):19-42. https://doi.org/10.4197/Ear. 23-2.2

Abd El-Naby HH, Saleh GM (2003) Radioelement distributions in the Proterozoic granites and associated pegmatites of Gabal El Fereyid area, Southeastern Desert, Egypt. *Appl Rad Isotopes* 59:289-299. https://doi.org/10.1016/j.apradiso.2003.07.002

Adabanija MA, Anie ON, Oladunjoye MA (2020) Radioactivity and gamma ray spectrometry of basement rocks in Okene area, southwestern Nigeria. NRIAG J Astron Geophys 9(1):71-8. https://doi.org/10.1080/20909977.2020.1711695

Adagunodo TA, Bayowa OG, Usikalu MR, Ojoawo AI (2019) Radiogenic heat production in the coastal plain sands of Ipokia, Dahomey Basin, Nigeria. *MethodsX* 6:1608-1616. https://doi.org/10.1016/j.mex.2019.07.006

Ademila O, Akingboye AS, Ojamomi AI (2018) Radiometric survey in geological mapping of parts of Basement Complex area of Nigeria. *Vietnam J Earth Sci* 40(3):288-298. https://doi.org/10.15625/0866-7187/40/3/12619

Ademola AK, Bello AK, Adejumobi AC (2014) Determination of natural radioactivity and hazard in soil samples in and around gold mining area in Itagunmodi, south-western, Nigeria. *J Rad Res Appl Sci* 7:249-255. http://dx.doi.org/10.1016/j.jrras.2014.06.001

Ademola AK, Hammed OS, Adejumobi CA (2008) Radioactivity and dose assessment of marble samples from Igbeti mines, Nigeria. *Rad Protection Dosimetry* 132(1):94-97. http://dx.doi.org/10.1093/rpd/ncn279

Ajayi IR, Adegbuyi O, Afolabi OM, Oniya EO (2006) Terrestrial gamma dose rates in Akoko, Southwestern Nigeria. *Sci Res Annals* 2(1):53-57.

Ajayi IR, Ajayi OS (1999) Estimation of absorbed dose rate and collective dose equivalent due to gamma radiation from selected radionuclides in soil in Ondo and Ekiti States, south-western Nigeria. *Rad Protection Dostimetry* 86(3)2:21-224.

Ajayi OS, Dike CG, Balogun KO (2018) Elemental and radioactivity analysis of rocks and soils of some selected sites in southwestern Nigeria. *Environ Forensic* 19(2):87-98.

Akingboye AS, Ademila O (2019) In situ natural radioactivity and radiological hazard assessments of granite gneiss outcrops in parts of the Southwestern Basement Complex of Nigeria. *J Nat Hazards and Environ* 5(2):1-11. https://doi.org/10.21324/dacd.475998

Akkurt I, Oruncak B, Gunoglu K (2010) Radioactivity and dose rates in commercially-used marble from Afyonkarahisar-Turkey. *Int J Phys Sci* 5(2):170-173.

Akpan AE, Ebong ED, Ekwok SE, Eyo JO (2020) Assessment of radionuclide distribution and associated radiological hazards for soils and beach sediments of Akwa Ibom Coastline, southern Nigeria. *Arab J Geosci* 13(15): 12p. https://doi.org/10.1007/s12517-020-05727-7

Al-Trabulsy HA, Khater AEM, Habbani FI (2011) Radioactivity levels and radiological hazard indices at the Saudi coastline of the Gulf of Aqaba. *Rad Phy Chem* 80(3):343-348. https://doi.org/10.1016/j.radphyschem.2010.09.002

Asfahani J, Aissa M, Al-Hent R (2007) Uranium migration in a sedimentological phosphatic environment in northern Palmyrides, Al-Awabed area, Syria. *Appl Rad Isotopes* 65:1078-1086. https://doi.org/10.1016/j.apradiso.2007.04.019

Avwiri GO, Nte FU, Olanrewaju AI (2011) Determination of radionuclide concentration of landfill at Eliozu, Port Harcourt, Rivers State. *Scientia Africana*, 10(1).

Bártová H, Kuceˇra J, Musílek L, Trojeck T, Gregorová E (2017) Determination of U, Th and K, in bricks by gamma-ray spectrometry, X-ray fluorescence analysis and neutron activation analysis. *Radiat Phys Chem* 140:161-166.

Bea F (1996) Residence of REE, Y, Th and U in granites and crustal protoliths; Implications for the chemistry of crustal melts. *J Petrol* 37:521-552.

Bea F (2012) The sources of energy for crustal melting and the geochemistry of heat-producing elements. *Lithos* 153:278-291. https://doi.org/10.1016/j.lithos.2012.01.017

Beretka J, Mathew PJ (1985) Natural radioactivity of Australia building materials, industrial wastes and by-products. *Health Phy*, 48:87-95. https://doi.org/10.1097/00004032-198501000-00007

Braun JJ, Pagel M, Herbillon A, Rosin C (1993) Mobilization and redistribution of REEs and thorium in a syenitic lateritic profile: a mass balance study. *Geochim Cosmochim Acta* 57:4419-4434. https://doi.org/10.1016/0016-7037(93)90492-F

Braun JJ, Viers J, Dupré B, Polve M, Ndam J, Muller J-P (1998) Solid/liquid REE fractionation in the lateritic system of Goyoum, East Cameroon: The implication for the present dynamics of the soil covers of the humid tropical regions. *Geochim Cosmochim Acta* 62:273-299. https://doi.org/10.1016/S0016-7037(97)00344-X

Chandrasekaran A, Ravisankar R, Senthilkumar G, Thillaivelavan K, Dhinakaran B, Vijayagopal P, Bramha SN, Venkatraman B (2014) Spatial distribution and lifetime cancer risk due to gamma radioactivity in Yelagiri Hills, Tamilnadu, India. *Egy J Basic Appl Sci* 1:38-48. http://dx.doi.org/10.1016/j.ejbas.2014.02.001

Chen J, Rahaman NM, Atiya IA (2010) Radon exhalation from building materials for decorative use. *J Environ Radioact* 101:317-322.

Cinar H, Altundas S, Çelik N, Maden N (2017) In situ gamma ray measurements for deciphering of radioactivity level in the Sarihan pluton area of northeastern Turkey. *Arab J Geosci* 10(19). https://doi.org/10.1007/s12517-017-3225-4

Cinelli G, Brattich E, Coletti C, De Ingeniis V, Mazzoli C, Mostacci D, Sassi R, Tositti L (2020) Terrestrial gamma dose rate mapping (Euganean Hills, Italy): comparison between field

measurements and HPGe gamma spectrometric data. *Radia Effects and Defects in Solids* 175:54-67. https://doi.org/10.1080/10420150.2020.1718131

Clauser C (2020) Radiogenic heat production of rocks.In: Gupta HK (ed), Encyclopedia of solid earth geophysics. *Encycl Earth Sci Series* 7p. https://doi.org/10.1007/978-3-030-10475-7_74-1

Coletti C, Brattich E, Cinelli G, Cultrone G, Maritan L, Mazzoli C, Mostacci D, Tositti L, Sassi R (2020) Radionuclide concentration and radon exhalation in new mix design of bricks produced reusing NORM by-products: The influence of mineralogy and texture. *Constr Build Mat* 260:119820. https://www.sciencedirect.com/science/article/pii/S0950061820318250

Constable JL, Hubbard FH (1981) U, Th and K distribution in a differentiated charnockite-granite intrusion and associated rocks from SW Sweden. *Miner Mag* 44:409-415.

Dickson BL, Scott KM (1997) Interpretation of aerial gamma-ray surveys – adding the geochemical factors. In: airborne magnetic and radiometric surveys. *J Austra Geol Geophys*, 17(2):187-200

Efimov AV (1978) Multiplikativnyj pokazatel dlja vydelenija endogennych rud po aerogammaspektrometriceskim dannym. In: Metody Rudnoj Geofiziki, edited by Naucno-proizvodstven Oje objedinenie "Geofizika" Leningrad.

Eggeling L, Genter A, Kölbel T, Münch W (2013) Impact of natural radionuclides on geothermal exploitation in the Upper Rhine Graben. *Geothermics*, 47:80-88. https://doi.org/10.1016/j.geothermics.2013.03.002

El Qassas RAY, Salaheldin M, Assran SAM, Fattah Th. A, Rashed MA (2020) Airborne gamma-ray spectrometric data interpretation on Wadi Queih and Wadi Safaga area, Central Eastern Desert, Egypt. NRIAG J Astron Geophys 9(1):155-167, https://doi.org/10.1080/20909977.2020.1728893

Eleraki ME, Ghieth B, Rahman NA, Zamzam S (2017) Hydrothermal Zones Detection Using Airborne Magnetic and Gamma Ray Spectrometric Data of Mafic/Ultramafic Rocks at Gabal El-Rubshi Area, Central Eastern Desert (CED), Egypt. *Adv Nat Appl Sci* 11(9):182-196.

El-Gamal A, Nasr S, El-Taher A (2007) Study of the spatial distribution of natural radioactivity in Upper Egypt Nile River sediments. *Rad Measurements* 42:457-465.

Elkhateeb SO, Abdellatif MAG (2018) Delineation of potential gold mineralisation zones in a part of Central Eastern Desert, Egypt using Airborne Magnetic and Radiometric data. *NRIAG J Astron Geophys* 7(2):361-376.

El-Sadek MA (2009) Radiospectrometric and magnetic signatures of a gold mine in Egypt. *J Appl Geophys* 67(1):34-43. https://doi.org/10.1016/j.jappgeo.2008.08.012

Erbek E, Dolmaz MN (2018) In situ measurements of radionuclide concentrations in south of Mulgacity, Turkey. *Environ Earth Sci* 77:366-377. https://doi.org/10.1007/s12665-018-7562-8

European Commission (EC) (1999) *Radiological Protection Principles concerning the Natural Radioactivity of Building Materials*. Radiation Protection 112.

Faweya EB, Oniya EO, Ojo FO (2013) Assessment of radiological parameters and heavy-metal contents of sediment samples from Lower Niger River, Nigeria. *Arab J Sci Engin* 38:1903-1908. https://doi.org/10.1007/s13369-013-0549-6

Gnojek I, Prichystal A (1985) A new zinc mineralisation detected by airborne gamma-ray spectrometry in northern Moravia, Czechoslovakia. *Geoexploration* 23:491-502.

Goodenough KM, Lusty PAJ, Roberts NMW, Key RM, Garba A (2014) Post-collisional Pan-African granitoids and rare metal pegmatites in western Nigeria: age, petrogenesis, and the 'pegmatite conundrum'. *Lithos* 200:22–34. https://doi.org/10.1016/j.lithos.2014.04.006

Hasterok D, Webb J (2017) On the radiogenic heat production of igneous rocks. *Geosci Frontiers* 8:919-940.

Hoover DB, Heran WD, Hill PL (1992) The geophysical expression of selected mineral deposit models. U.S. Geological Survey Open-File report 92-557.

IAEA (1991) *Airborne gamma ray spectrometer surveying*. *International Atomic Energy Agency*. Technical Report Series, No. 323.

IAEA (2003) *Radiation protection and the management of radioactive waste in the oil and gas industry*. International Atomic Energy Agency. 173 p.

ICRP (1977) *Recommendations of the International Commission on Radiological Protection (ICRP)*. Pergamon Press, New York. 87 p.

ICRP (1990) *Recommendations of the International Commission on Radiological Protection (ICRP)*. Pergamon Press, New York. ICRP Pub. 60.

Innocent JA, Onimisi MY, Jonah SA (2013) Evaluation of naturally occurring radionuclide materials in soil samples collected from some mining sites in Zamfara state, Nigeria. *British J Appl Sci Technol* 3(4):684-692.

Kalyoncuoglu UY (2015) In situ gamma source radioactivity measurement in Isparta plain, Turkey. *Environ Earth Sci* 73:3159-3175. https://doi.org/10.1007/s12665-014-3610-1

Kathren RL (1998) NORM sources and their origins. *Appl Rad Isotopes* 49(3):149-168. https://doi.org/10.1016/S0969-8043(97)00237-6

Killeen PG, Heier KS (1974) Variation in the Levang Granite-Gneiss, Bamble Region South Norway. *Contrib Mineral Petrol 48*:171-177.

Killeen PG, Heier KS (1975) A uranium and thorium enriched province of the Fennoscandian shield in southern Norway. *Geochimica et Cosmochlmica Acta* 39:1515-1524.

Kroner A, Ekwueme BN, Pidgeon RT (2001) The Oldest Rocks in West Africa: SHRIMP Zircon Age for Early Archean Migmatitic Orthogneiss at Kaduna, Northern Nigeria. *The J Geol* 109:399-406. https://doi.org/10.1086/319979

Maden N, Akaryali E (2015a) Gamma ray spectrometry for recognition of hydrothermal alteration zones related to a low sulfidation epithermal gold mineralisation (eastern Pontides, NE Türkiye). *J Appl Geophys* 122:74-85. http://dx.doi.org/10.1016/j.jappgeo.2015.09.003

Maden N, Akaryali E (2015b) A review for genesis of continental arc magmas: U, Th, K and radiogenic heat production data from the Gümüşhane Pluton in the Eastern Pontides (NE Türkiye). *Tectonophys* 664:225-243. https://doi.org/10.1016/j.tecto.2015.09.023

Mamont-Ciesla K, Gwiazdowski B, Biernacka M, Zak A (1982) Radioactivity of building materials in Poland. In: Vohra G, Pillai KC, Sadavisan S, (edn.). *Natural radiation environment.* New York: Halsted Press. 551 p.

Mareschal JC, Jaupart C, Gariépy C, Cheng LZ, Guillou-Frottier L, Bienfait G, Lapointe R (2000) Heat flow and deep thermal structure near the southeastern edge of the Canadian Shield. *Can J Earth Sci* 37:399-414. https://doi.org/10.1139/e98-106

Narayana Y, Shetty PK, Siddappa K (2005) Enrichment of natural radionuclides in monazite areas of coastal Kerala. *Int Congress Series* 1276:333-334. https://doi.org/10.1016/j.ics.2004.11.163

Nisbet H, Migdisov AA, Williams-Jones AE, Xu H, van Hinsberg VJ, Roback R (2019) Challenging the thorium-immobility paradigm. Scientific Reports 9, 17035. https://www.nature.com/articles/s41598-019-53571-x

Ogunyele AC, Oluwajana OA, Ehinola IQ, Ameh BE, Salaudeen TA (2019). Petrochemistry and petrogenesis of the Precambrian Basement Complex rocks around Akungba-Akoko, southwestern Nigeria. *Materials and Geoenviron* 66(3): 173-184. https://doi.org/10.2478/rmzmag-2019-0036

Oxburg ER (1980) Heat flow and magma genesis. In: Hargraves RB (Ed.), Physics of Magmatic Processes. Princeton University Press, New Jersey, pp. 161-199.

Oyeyemi KD, Usikalu MR, Aizebeokhai AP, Achuka JA, Jonathan O (2017) Measurements of radioactivity levels in part of Ota Southwestern Nigeria: Implications for radiological hazards indices and excess lifetime cancer-risks. *IOP Conference Series: J Phys* 852:1-8. https://doi.org/10.1088/1742-6596/852/1/012042

Perry HKC, Jaupart C, Mareschal J, Bienfait G (2006) Crustal heat production in the Superior Province, Canadian Shield, and in North America inferred from heat flow data. *J Geophys Res: Solid Earth* 111:1-20. https://doi.org/10.1029/2005JB003893

Portnov AM (1987) Specialization of rocks toward potassium and thorium in relation to mineralisation. *Int.Geol Rev* 29:326-344.

Rafique M, Rahman SU, Basharat M, Aziz W, Ahmad I, Lone KA, Ahmad K, Matiullah (2014) Evaluation of excess life time cancer risk from gamma dose rates in Jhelum valley. *J Rad Res Appl Sci* 1-7. http://dx.doi.org/10.1016/j.jrras.2013.11.005

Rahaman MA (1989) Review of the Basement Geology of Southwestern Nigeria. In: Kogbe C A (eds.). *Geology of Nigeria* (2nd eds.). Rockview Nigeria Limited, Jos. 39-56.

Ramasamy V, Suresh G, Meenakshisundaram V, Gajendran V (2009) Evaluation of natural radionuclide content in river sediments and excess lifetime cancer risk due to gamma radioactivity. *Res J Environ Earth Sci* 1(1):6-10.

Ramasamy V, Suresh G, Meenakshisundaram V, Ponnusamy V (2011) Horizontal and vertical characterisation of radionuclides and minerals in river sediments. *Appl Rad Isotopes* 69 (1):184-195. https://doi.org/10.1016/j.apradiso.2010.07.020

Ramola RC, Manjulata Y, Gusain GS (2014) Distribution of natural radionuclide along Main Central Thrust in Garhwal Himalaya. *J Rad Res Appl Sci* 7(4):614-619. https://doi.org/10.1016/j.jrras.2014.10.002

Rosianna I, Nugraha ED, Syaeful H, Putra S, Hosoda M, Akata N, Tokonami S (2020) Natural radioactivity of laterite and volcanic rock sample for radioactive mineral exploration in Mamuju, Indonesia. *Geosci* 10:376. https://doi.org/10.3390/geosciences10090376

Rudnick RL, Fountain DM (1995) Nature and composition of the continental crust: a lower crustal perspective. *Rev Geophys* 33:267-309.

Rybach L (1988) Determination of the heat production rate. In: Haenel R, Rybach L, Stegena L (eds) *Handbook of Terrestrial Heat-Flow Density Determination*. Kluwer Academic Publishers, Dordrecht. 125-142.

Sabra MEM, Abdeldayem AL, Youssef MAS, Masoud AA, Mansour SA (2019) Determination of the radiation dose rate and radiogenic heat production of North Gabal Abu Hibban area, central Eastern Desert, Egypt. *NRIAG J Astron Geophys*, 8(1):103-111. https://doi.org/10.1080/20909977.2019.1617556

Saqan SA, Kullab MK, Ismail AM (2001) Radionuclides in hot mineral spring waters in Jordan. *J Environ Radio* 52(1):99-107. https://doi.org/10.1016/S0265-931X(00)00096-5

Schmucker U (1969) Geophysical aspects of structure and composition of the Earth. In: Wedepohl KH (Ed.), Handbook of Geochemistry (I). Springer-Verlag, Berlin. pp. 134-226.

Smithson SB, Decker ER (1974) A continental crustal model and its geothermal implications. *Earth Planet Sci Lett* 22(3):215-225.

Stoulos S, Manolopoulou M, Papastefanou C (2003) Assessment of natural radiation exposure and radon exhalation from building materials in Greece. *J Environ Radioact* 69:225-240.

Tan G, Li C, Li M, (1991) Investigation of environment natural penetrating radiation level in Guangdong Province. *Rad Protection (in Chinese with English abstract)* 11:47-57.

Taskin H, Karavus M, Ay P, Topuzoglu A, Hindiroglu S, Karahan G (2009) Radionuclide concentrations in soil and lifetime cancer risk due to gamma radioactivity in Kirklareli, Turkey. *J Environ Radio* 100(1):49-53. https://doi.org/10.1016/j.jenvrad.2008.10.012

Tufail M, Nasim-Akhar Sabiha-Javied SA, Hamid T (2007) Natural radiation hazard in building bricks fabrication from soils of two districts of Pakistan. *J Radio Protection* 27:481-492. https://doi.org/10.1088/0952-4746/27/4/009

Tzortzis M, Tsertos H (2004) Determination of uranium, thorium and potassium elemental concentration in surface soils in Cyprus. *J Environ Radio* 77(3):325-338. https://doi.org/10.1016/j.jenvrad.2004.03.014

Tzortzis M, Tsertos H, Christofides C, Christodoulides G (2003) Gamma radiation measurement and dose rates in commercially-used natural tiling rocks (granites). *J Environ Radio* 70(1):223-235. https://doi.org/10.1016/S0265-931X(03)00106-1

UNSCEAR (1988) *Sources, effects and risks of ionizing radiation*. United Nations Scientific Committee on Effect of Atomic Radiation (UNSCEAR), United Nations, New York. 647 p.

UNSCEAR (1993) *Sources and effects of ionizing radiation*. United Nations Scientific Committee on Effect of Atomic Radiation (UNSCEAR), United Nations, New York. 920 p.

UNSCEAR (2000) *Exposure from natural radiation source*. United Nations Scientific Committee on Effect of Atomic Radiation (UNSCEAR), Report to general assembly. Annex B, United Nations, New York, 1-2, 76 p.

Uyanık NA, Uyanık O, Gür F, Aydın İ (2013) Natural radioactivity of bricks and brick material in the Salihli-Turgutlu area of Turkey. *Environ Earth Sci* 68(2):499-506. https://doi.org/10.1007/s12665-012-1754-4

Wang Q, Song J, Li X, Yuan H, Li N, Cao L (2016) Environmental evolution records reflected by radionuclides in the sediment of coastal wetlands: a case study in the Yellow River Estuary wetland. *J Environ Radioact* 162-163:87-96.

Woakes M, Rahaman MA, Ajibade AC (1987) Some Metallogenetic Features of the Nigerian Basement. *J Afri Earth Sci* 6(5):655-664. https://doi.org/10.1016/0899-5362(87)90004-2

Wollenberg HA, Smith AR (1987) Radiogenic heat production of crustal rocks: an assessment based on geochemical data. *Geophys Res Lett* 14(3):295-298.

Xinwei L, Lingqing W, Xiaodan J (2006) Radiometric analysis of Chinese commercial granites. *J Radioanalytical Nuclear Chem*, 267(3):669-673. https://doi.org/10.1007/s10967-006-0101-1

Youssef MAS (2016) Estimating and interpretation of radioactive heat production using airborne gammaray survey data of Gabal Arrubushi area, Central Eastern Desert, Egypt. *J Afr Earth Sci.* https://doi.org/10.1016/j.jafrearsci.2015.10.022

Youssef MAS, Elkhodary ST (2013) Utilization of airborne gamma ray spectrometric data for geological mapping, radioactive mineral exploration and environmental monitoring of southeastern Aswan city, South Eastern Desert, Egypt. *Geophys J Int* 195(3):1689-1700. https://doi.org/10.1093/gji/ggt375

Youssef MAS, Sarab MEM, Abdeldayem AL, Masoud AA, Mansour SA (2017) Uranium migration and favourable sites of potential radioelement concentrations in Gabal Umm Hammad area, Central Eastern Desert, Egypt. *NRIAG J Astron Geophys* 6:368-378.

Zhu XK, O'Nions RK (1999) Monazite chemical composition: some implications for monazite geochronology. *Contrib Mineral Petrol* 137:351-363.